Science of the Total Environment 731 (2020) 139176

Contents lists available at ScienceDirect

Science of the Total Environment

journal homepage: www.elsevier.com/locate/scitotenv

Isotopic constraints on water balance of tundra lakes and watersheds affected by permafrost degradation, Mackenzie Delta region, Northwest Territories, Canada

Chengwei Wan [a,b,c], John J. Gibson [b,c,*], Daniel L. Peters [b,d]

[a] State Key Laboratory of Hydrology - Water Resources and Hydraulic Engineering, Hohai University, Nanjing 210098, China
[b] Department of Geography, University of Victoria, P.O. Box 3060 STN CSC, Victoria, BC 11 V8W 2Y2, Canada
[c] InnoTech Alberta, 3- 4476 Markham Street, Victoria, BC V8Z 7X8, Canada
[d] Watershed Hydrology & Ecology Research Division, Water Science and Technology Directorate, Environment and Climate Change Canada, University of Victoria, P.O. Box 3060 STN CSC, Victoria, BC 11 V8W 3R4, Canada

HIGHLIGHTS

- Isotope balance used to interpret new ^{18}O and ^{2}H data from 60 thermokarst lakes
- Corrections applied for seasonal volume changes and continental-marine air mixing
- Evaporation/inflow, precipitation/inflow, water yield and runoff ratios estimated
- Water balance trends found to be driven by climate gradients and thaw trajectory
- Systematic runoff responses also found for shoreline thaw slumping and wildfire

GRAPHICAL ABSTRACT

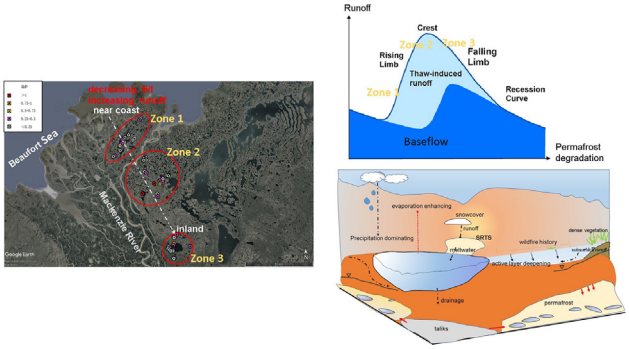

ARTICLE INFO

Article history:
Received 28 November 2019
Received in revised form 27 April 2020
Accepted 1 May 2020
Available online 05 May 2020

Editor: Jürgen Mahlknecht

Keywords:
Thermokarst lakes
Permafrost
Thaw slumps
Isotope mass balance
Mackenzie delta region

ABSTRACT

Widespread permafrost degradation in Canada's western Arctic has led to formation of shoreline retrogressive thaw slumps (SRTS), a process influential in modifying water and biogeochemical balances of tundra lakes. To investigate hydrological effects of SRTS, water sampling campaigns were conducted in 2004, 2005, and 2008 for paired lakes (undisturbed vs SRTS) in the upland region adjacent to the Mackenzie Delta, Northwest Territories, Canada. An isotope mass balance model to estimate evaporation/inflow, precipitation/inflow, water yield, and runoff ratio was developed incorporating seasonal evaporative drawdown effects and a mixing model to simulate gradients in marine-continental atmospheric moisture. Site-specific water balance results revealed systematically higher evaporation/inflow and precipitation/inflow for lakes with active SRTS compared to undisturbed lakes, and typically higher ratios of these indicators associated with stabilized versus active SRTS. Water yields were higher for active SRTS sites compared to undisturbed and stabilized SRTS sites, suggesting that slumping is an initial but not a sustained source of water delivery to lakes. Catchments with wildfire history were found to have lower water yields, attributed to reduced permafrost influence on runoff generation. Conceptually, we define a permafrost thaw trajectory whereby undisturbed sites, active SRTS, stabilized SRTS, and ancient SRTS represent progressive stages of permafrost thaw. We postulate that release of additional runoff is mainly due to permafrost thaw in active SRTS, which also promotes lake expansion, talik formation, and subsurface

* Corresponding author at: Department of Geography, University of Victoria, P.O. Box 3060 STN CSC, Victoria, BC 11 V8W 2Y2, Canada.
E-mail address: jjgibson@uvic.ca (J.J. Gibson).

https://doi.org/10.1016/j.scitotenv.2020.139176

connectivity. Eventual stabilization of slumps and reduced runoff is expected once permafrost thaw sources are exhausted, at which time lakes may become more reliant on replenishment by direct precipitation. The effect of snow catch in slumps appears to be subordinate to permafrost thaw sources based on eventual decline in runoff once thaw slumps stabilize. Improved, site-specific hydrologic understanding is expected to assist with ongoing research into carbon cycling and biogeochemical feedbacks in the region.

1. Introduction

Global warming over the past century, especially during the summer months, has led to widespread permafrost degradation across high-latitudes areas (Box et al., 2019; Pavlov, 1994; Hinzman et al., 2005; Liljedahl et al., 2016). Over the past few decades, an increase in the number of occurrences and areal extent of terrain disturbances have been observed, including deepening of the active layer, thawing of ice wedges, and local ground subsidence, all of which can be further enhanced by the occurrence of wildfire (Lantz and Kokelj, 2008; Kokelj et al., 2015; Lantz and Turner, 2015). Thermokarst processes, including melting of ground ice causing land surface subsidence, has particularly affected landscapes underlain by ice-rich permafrost, initiating formation and expansion of thaw lakes and slumps in the northwestern Arctic regions of North America (Kokelj and Jorgenson, 2013; Karlsson et al., 2013). Retrogressive thaw slump activity is a widespread occurrence across these regions, and is measurably increasing (Lantz and Kokelj, 2008; Lacelle et al., 2009; Lewkowicz and Way, 2019). Similarly affected regions include the Russian Arctic, Siberia, and Qinghai-Tibet Plateau (Séjourné et al., 2015; Balser et al., 2014; Luo et al., 2019).

In the lake-rich upland area adjacent to the Mackenzie Delta, Northwest Territories, Canada, which are known to be hydologically isolated from riverine influence and seawater interaction (Kokelj et al., 2005, 2009: Burn and Kokelj, 2009), the most prominent permafrost degradation features are retrogressive thaw slumps, which mainly develop on slopes adjacent to lake shores. Permafrost in the area is continuous and several hundred metres thick in coastal areas with tundra vegetation, transitioning southward to discontinuous permafrost in areas with tall shrubs and spruce forest where ground temperatures may be several degrees warmer (Kokelj et al., 2017). Slumps are generally active for 30 to 50 years, although slump size, as controlled by rates of backwasting of ice-rich headwall material, can vary greatly (Lacelle et al., 2009). It has been estimated that around 10% of lakes >1 ha have been affected by the growth of shoreline retrogressive thaw slumps (SRTS) and that SRTS activity, number, and areal extent has accelerated since the 1950s (Lantz and Kokelj, 2008).

SRTS influences hydrological and environmental processes in tundra lakes, not only by directly eroding and collapsing shorelines, leading to release of material downslope to lakes, but thermally, by altering soil conditions and thereby mobilizing water, solutes, and biological materials and promoting transport and interaction with freshwater environments (Abbott et al., 2014, 2015; Lantuit et al., 2012; Lacelle et al., 2015; Kokelj et al., 2015). Previous studies have identified significant changes in limnology (Kokelj et al., 2005, 2009; Thompson et al., 2012; Houben et al., 2016), biological behavior (Mesquita et al., 2010; Thienpont et al., 2013), and water contaminants (Deison et al., 2012; Eickmeyer et al., 2016) in lakes impacted by SRTS in uplands adjacent to the Mackenzie Delta. For instance, notably higher major-ion and lower DOC concentrations, as well as shifts in nutrients, light and phytoplankton relationships have been observed in SRTS impacted lakes compared with unimpacted lakes (Kokelj et al., 2005; Thompson et al., 2012; Houben et al., 2016).

Prior studies in this region have provided considerable insight into geochemical and biological processes (Kokelj et al., 2005; Lantz and Kokelj, 2008; Thompson et al., 2012; Houben et al., 2016), although the study of hydrological processes in SRTS affected lake basins has received less attention (Vonk et al., 2015). One exception is the study by Marsh et al. (2009), who described catastrophic drainage of thermokarst lakes via melting of ice wedges and creation of new lake outflows. Little work has been carried out on potentially important changes to hydrological processes and lake water balances resulting from the formation and evolution of SRTS.

Previous investigations carried out in the cold regions have used isotope mass balance (IMB) methods to assess water balance of lakes (Gibson et al., 1993; Gibson and Edwards, 2002), including thermokarst lakes (Turner et al., 2010, 2014; Tondu et al., 2013; Anderson et al., 2013; Arp et al., 2015; Narancic et al., 2017). Considering the logistical difficulties associated with long-term, physically-based monitoring in remote areas, the application of site-specific IMB offers a practical alternative for characterization of regional hydrology across lake-rich landscapes with pronounced environmental gradients (Gibson et al., 2016a; MacDonald et al., 2016; Bouchard et al., 2017; Wan et al., 2019). Presence of lakes is advantageous when applying IMB in low-time frequency surveys as these water bodies serve as an archive of lake and watershed hydrological processes integrated over the residence time of water in the system, thereby providing a longer-term record of water balance exchanges.

Capitalizing on available field-based measurements from a carefully planned series of paired lakes studies (e.g. Kokelj et al., 2005, 2009), and by piggy-backing on various water sampling campaigns designed mainly for biogeochemical studies (e.g. Thompson et al., 2012), we were able to accrue an isotopic dataset including ^{18}O and ^{2}H signatures for paired lakes catchments (reference vs SRTS affected) along a latitudinal transect in the upland region adjacent to the Mackenzie Delta during the end of summer of 2004, 2005, and 2008.

The objectives of this paper, which focuses on hydrological information gained from ^{18}O and ^{2}H, are as follows: 1) to provide a description of the isotopic dataset and describe basic controls on isotopic labelling of waters in the region including lakes and input sources; 2) to develop an IMB model for assessing water balance conditions and relative hydrological characteristics across the subarctic boreal forest-tundra transition; 3) to calculate hydrological indicators including evaporation/inflow, precipitation/inflow, water yield, and runoff ratios to quantify and illustrate site-specific water balance variations in lake pairs and across the landscape; and, 4) to explore the influence of permafrost disturbance on lake and catchment water balance. As described herein, this study was designed to provide an improved, quantitative understanding of tundra lake hydrology in a permafrost region experiencing SRTS activity, and to advance current conceptual models of these processes.

2. Study area

The study area is located in the uplands east of the Mackenzie River Delta, northwestern Canada, near Inuvik. Studies were conducted along a northwest-southeast transect from treeless/low-shrub tundra near the Beaufort Sea coast at Richards Island to brush tundra mixed with boreal forest near Inuvik (Ritchie, 1984; Timoney et al., 1992; Burn, 1997; Lantz et al., 2013) (Fig. 1). The uplands study lakes are not affected by water flow or ice jam processes related to the Mackenzie River, and the majority of these lakes were selected due to their first order location within headwater catchments.

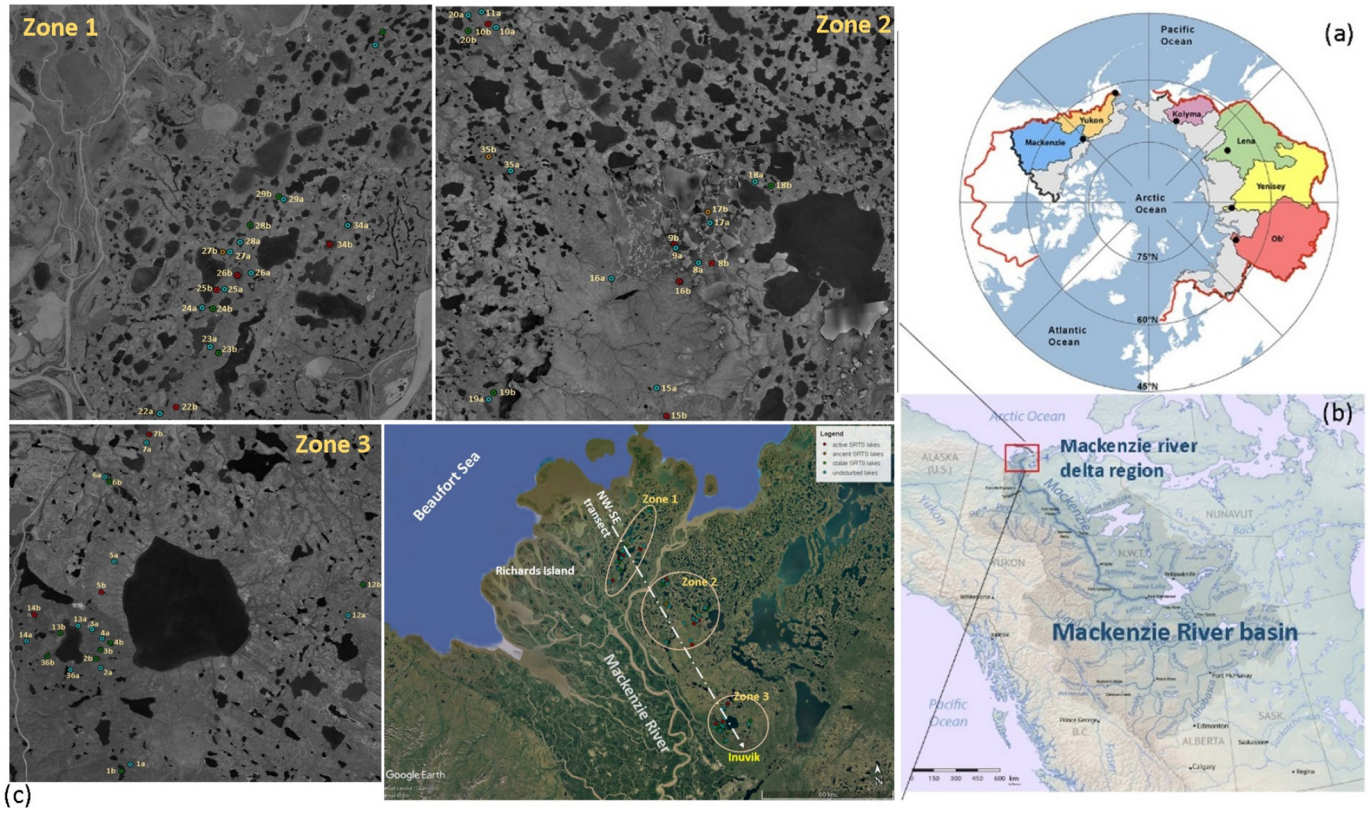

Fig. 1. (a) Six major river watersheds in the pan-arctic area: Yenisey, Lena, Ob', Mackenzie, Yukon and Kolyma from Mann et al. (2016), (b) Mackenzie River Basin, Canada, showing the Mackenzie River delta region (red box), (c) Satellite images showing position of study lakes along the NW-SE transect from the Beaufort Sea coast to Inuvik, Northwest Territories, Canada. The paired-lake study design compares reference lakes to disturbed lakes, including lakes with active, stable and ancient shoreline retrogressive thaw slumps (SRTS), as classified by Houben et al. (2016). (For interpretation of the references to colour in this figure legend, the reader is referred to the web version of this article.)

Surficial materials in the area consist of Quaternary deposits derived from carbonate and shale bedrock sources within the Mackenzie Basin (Rampton, 1988). The terrain is characterized by rolling tundra underlain by continuous permafrost, with taliks underlying most areas where lake or river ice does not freeze to the bottom in winter (Burn, 2002; Kokelj et al., 2005, 2009). Permafrost thicknesses can reach up

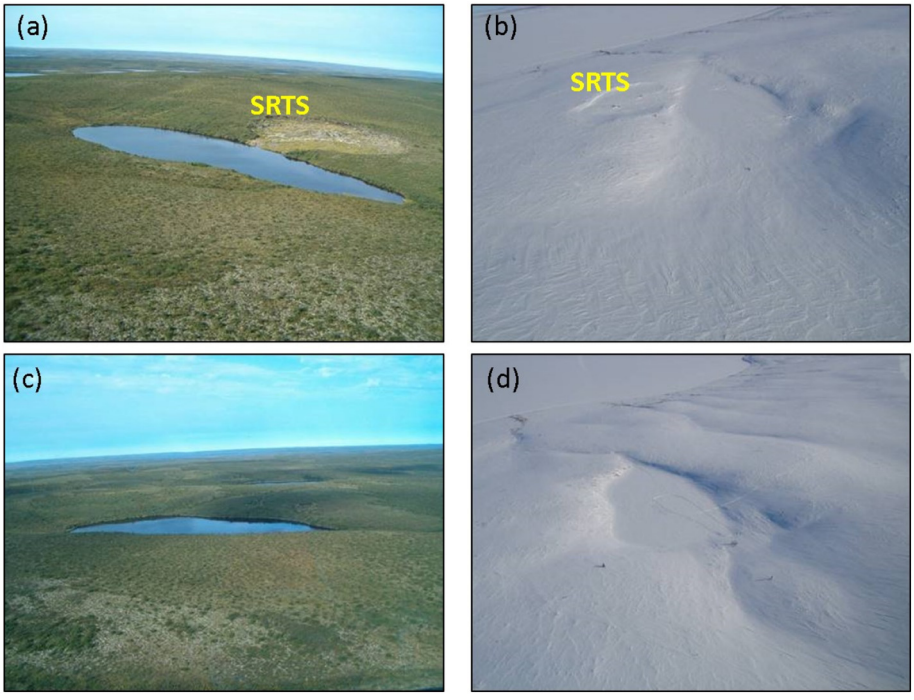

Fig. 2. Tundra lakes in Zone 3. Lake 5b with an active shoreline retrogressive thaw slump (SRTS) in (a) September 2004, and (b) May 2006; and Lake 5a (undisturbed) in (c) September 2004, and (d) May 2006.

to several hundred metres, with an active layer typically ranging from 35 to 85 cm in depth (Burn and Kokelj, 2009). The ice-rich (> 80%) permafrost contains numerous ice-wedge polygons, with common occurrences of ground (massive) ice exposed in retrogressive thaw slumps and pingos (Rampton, 1988; Kokelj et al., 2009).

Thermokarst activity in the vicinity has increased in the last 40 years, resulting in creation of innumerable lakes and ponds (Lantz and Kokelj, 2008). Thawing of ice-rich permafrost on sloping terrain has promoted the development of SRTS (Kettles and Tarnocai, 1999; Lantz and Kokelj, 2008; Burn and Kokelj, 2009; Kokelj et al., 2009) (Fig. 2). Active layer deepening, thawing of near-surface massive segregated ice, and thermokarst formation have also been enhanced by wildfire occurrences since the 1960s (Mackay, 1995; Kokelj et al., 2009). For instance, an extensive area around Inuvik and north to Noell Lake was affected by wildfire in 1968, which destroyed surface organic materials causing active-layer deepening, thawing of ice-rich permafrost, and release of water and nutrients to the base of the active layer (Kokelj et al., 2005).

Significant climatic gradients occur in the region along the study transect from coastal to inland areas with three distinct zones (Fig. 1). Mean annual air temperature ranges from −10.1 (Zone 1) to −8.1 °C (Zone 3); mean annual precipitation ranges from 161 (Zone 1) to 241 mm (Zone 3) (Tuktoyaktuk and Inuvik Stations, respectively; Environment and Climate Change Canada, 2019). Positive gradients in mean annual evaporation and decreasing mean annual humidity are also noted moving away from the Beaufort marine vapor influence (Fig. S1, Table S1). Zonal weather conditions for the three sampling years (2004, 2005, & 2008), and wet/dry status compared to long-term means (1979–2008) are also provided based on interpolation from the North American Regional Reanalysis dataset (Table S1). Overall, zonal gradients in mean annual air temperature, annual evaporation and relative humidity were + 1.5 °C, +63 mm, and v-4.1%, respectively, with slightly higher annual precipitation inland (+19 mm) and lower P-E (−144 mm), where P-E is precipitation (P) minus open-water evaporation (E). Climate gradients based on NARR (Mesinger et al., 2006) show similar trends to the station-based climate records, suggesting warmer and drier conditions with distance from the coast. It is important to note that lower mean annual air temperature and evaporation in Zone 1 is partly attributed to persistence of sea ice into the summer months.

Among the study years, we note that 2004 was a cold and dry year for all three zones (Fig. S1), while the annual evaporation was similar or above average conditions for most sites in the area. In comparison, warmer conditions in 2005 and 2008, which are recognized as wet years, had greater than average precipitation amounts (>300 mm). Reduced relative humidity in 2008 compared to 2005 may also have been affected by antecedent moisture conditions, given that recorded precipitation in the previous year was extremely low (83 to 87 mm less than average). Colder air temperature and higher precipitation may also have contributed to lower evaporation totals in 2008 as compared to 2005. For the most part, positive P–E values, and systematic climate gradients were recorded throughout 2004 to 2008. Spatially, based on the NARR dataset, P-E ranged from 90 to 230 mm in Zone 1, 40 to 190 mm in Zone 2, and 30 to 140 mm in Zone 3 over the entire study period. However, negative P-E values were recorded in inland areas (Zone 3) during the dry years, where evaporation typically exceeded precipitation by 30 to 50 mm (15 to 25%).

3. Materials and methods

3.1. Field surveys

Kokelj et al. (2005, 2009) initiated the uplands lakes study which identified 60+ lakes along a transect from Richards Island to Inuvik for investigation of the effects of permafrost degradation on lake geochemistry (Fig. 1). This 100+ km transect has also enabled the assessment of environmental effects such as marine coastal influence, proximity to treeline, and recent fire history.

A total of 32 lake pairs were identified based on similarity factors (morphometry, geology) and geographical proximity. Lake pairs are grouped by number, with reference lakes denoted by the suffix “a” and SRTS-affected lakes denoted by the suffix “b” (Kokelj et al., 2005, 2009). SRTS types are classified as active, stable, or ancient (Table S2). Active SRTS (13 sites) are characterized by presence of bare areas, exposed ground ice, steep thawing headwalls, and little vegetation growing within the thaw slump scar. Stable SRTS (16 sites) are predominantly vegetated (coverage > 50%) with shallow, inactive headwalls. Ancient SRTS (3 sites) are characterized by subdued headwall relief and fully-vegetated, tundra foot slopes (Kokelj et al., 2009).

The selected lakes are predominantly headwater lakes with regionally representative lake surface areas (LA) ranging from 0.5 to 116.5 ha (Kokelj et al., 2005, 2009; Houben et al., 2016). A few lakes were subsequently found to be potentially receiving outflow from another lake. Catchment areas (CA) range from 1.6 to 22 times lake area. SRTS footprint ranges from 1 to 37% of the catchment area (Table S2). Reference (undisturbed) lakes are generally smaller in area than active/stable SRTS affected lakes (disturbed lakes), but share larger CA/LA ratios. Active SRTS lakes have greater lake and catchment areas than other lakes, and their slump areas are positively correlated to lake and catchment sizes (Table S3). Stable SRTS lakes have the smallest CA/LA ratios, and they share smaller thaw slump areas (ranging from 0.6 to 4.9 ha) as compared to active SRTS lakes, which range from 0.8 to 15.3 ha. 8 of 32 reference lakes, 2 of 13 SRTS disturbed lakes, and 7 of 16 stable SRTS disturbed lakes have a history of wildfire (see Kokelj et al., 2005).

3.2. Water sampling and analysis

During late August/early September 2004 and 2005, and early October 2008, select upland tundra lakes were sampled near the lake centre at 0.5 m depth below water surface and transferred to tightly sealed 30 ml HDPE bottles with minimal head space for ^{18}O and ^{2}H analyses. Whenever possible, surface runoff was also collected from undisturbed inflow areas, disturbed slump areas, and channelized lake outflows. Two ground ice samples were also collected at slump headwall sites in catchments of Lakes 9b and 11b in September 2004. In 2010, subsurface soil water was also sampled on slopes adjacent lakes 5a and 5b. Summer rainfall was collected in bulk samplers with mineral oil added to prevent evaporation, and snowpack samples were also collected along representative transects in the watersheds during late winter.

The areal extent of thaw slumping was similar in all three zones (i.e. Zone 1: 8.7%; Zone 2: 7.4%; Zone 3: 9.9%). Zones 2 (4 lake pairs) and 3 (7 pairs) were visited in 2004 by Kokelj et al. (2005, 2009) and Thompson et al. (2012). The number of sites increased to 10 pairs in each of the three zones in 2005. While in 2008, 5 pairs in Zone 1 and 10 pairs in Zones 2 and 3 were accessed. A total 92 lake water samples were collected, along with select rainfall (12), snow (116), inflow (22), slump water (19) that were either inflowing or pooled, as well as channelized lake outflows (31).

Water samples were analyzed for $\delta^{2}H$ and $\delta^{18}O$ by conventional isotope ratio mass spectrometry at the Environmental Isotope Lab, University of Waterloo in 2004 and then at G.G. Hatch Stable Isotope Laboratory, University of Ottawa in 2005 and 2008. Both labs had regularly participated in inter-comparison tests to ensure compatibility of results with international standards (e.g. IAEA, 2011). Results are presented in δ notation in per mil (‰) relative to Vienna Standard Mean Ocean Water (V-SMOW). Analytical uncertainty based on standard deviation of repeats is better than 0.1‰ for $\delta^{18}O$ and 1‰ for $\delta^{2}H$, respectively.

3.3. Isotope mass balance

Water samples, classified by type, were initially plotted in $\delta^{18}O$ - $\delta^{2}H$ space (Fig. 3) and referenced to the Global Meteoric Water Line (GMWL) of Craig (1961) and a Local Meteoric Water Line (LMWL) based on 1986–1998 monthly records for Inuvik accessed from the Global Network for Isotopes in Precipitation (GNIP) database (Birks et al., 2002). The LMWL was approximated based on regression of amount-weighted monthly averages for the period of record. Customized $\delta^{18}O$ - $\delta^{2}H$ frameworks were created to illustrate zonal and interannual variations in both lake water enrichment patterns and input sources to lakes (Fig. 4). Observed local evaporation lines (LEL) based on simple regression of single lake water analyses, and predicted isotopic enrichment trends based on theoretical considerations (described below) are shown for each case (Fig. 4).

Isotope mass balances were developed to describe site-specific hydrology of individual lakes based on the observed isotopic enrichment of lake water compared to input sources. Isotopic enrichment is attributable to the effect of open-water evaporation from the lake. The basic theory describing this effect, which relies on the Craig and Gordon (1965) model, has been widely applied in such lake surveys to predict isotopic enrichment and to estimate evaporation losses as a component of inflows (e.g. Gibson et al., 2016a; Wan et al., 2019). In this study, we apply a non-steady variant of the basic IMB model which accounts not only for evaporation, inflow and outflow, but also for seasonal volumetric drawdown of lake water by evaporation, as utilized previously for cold regions lakes by Gibson (2002). This model set-up was found to be more realistic in predicting isotopic enrichment in the study lakes, which in some cases were highly evaporative and typically did not maintain a constant volume during the peak evaporation season. Under the assumption that the lakes were shallow and well-mixed at time of sampling, and that the isotopic composition of precipitation (δ_P) was adequately representative of total input during the ice-free period (δ_I), (i.e. $\delta_P = \delta_I$) the water mass and isotope mass balance equations for the evaporation period are:

$$\frac{dV}{dt} = I - E \tag{1}$$

$$V\frac{d\delta_L}{dt} + \delta_L\frac{dV}{dt} = I\delta_I - E\delta_E \tag{2}$$

where V is the volume of lake, t is the time, dV is the change in volume over time interval dt, E is the evaporation and δ_E is the Craig and Gordon (1965) model isotopic composition of evaporative flux:

$$\delta_E = ((\delta_L - \varepsilon^+)/\alpha^+ - h\delta_A - \varepsilon_K)/\left(1 - h + 10^{-3}\varepsilon_K\right) \tag{3}$$

where ε^+ is the equilibrium isotopic separation (Horita and Wesolowski, 1994), α^+ is the equilibrium isotopic fractionation, where $\varepsilon^+ = \alpha^+ - 1$, and ε_K is the kinetic isotopic separation (Horita et al., 2008), where

$$\alpha^+\left({}^{18}O\right) = \exp[-7.685/10^{-3} + 6.7123/(273.15 + T) - 1666.4/(273.15 + T)^2 + 350410/(273.15 + T)^3]) \tag{4}$$

$$\alpha^+\left({}^{2}H\right) = \exp\left[1158.8(273.15 + T)^3/10^{12}\right) - 1620.1 \times \left((273.15 + T)^2/10^9\right) + 794.84\left((273.15 + T)/10^6\right) - 161.04/10^3 + 2999200/(273.15 + T)^3] \tag{5}$$

If we define the remaining fraction of lake water as:

$$f = V/V_0 \tag{6}$$

where V is the residual volume and V_0 is the original volume;

Then integrating Eqs. (1), (2) and (6) and the equation of isotopic and hydrologic steady state described by Gibson et al. (2016a) and noting that $df = dV/V_0 = (I - E) \cdot dt/V_0$, the annual water loss by evaporation (x) can be estimated as:

$$x = E/I = \left[\delta_I - \frac{\delta_L - \delta^*}{f^m} - \delta^*\right]/\left(\delta_E - \frac{\delta_L - \delta^*}{f^m} - \delta^*\right) \tag{7}$$

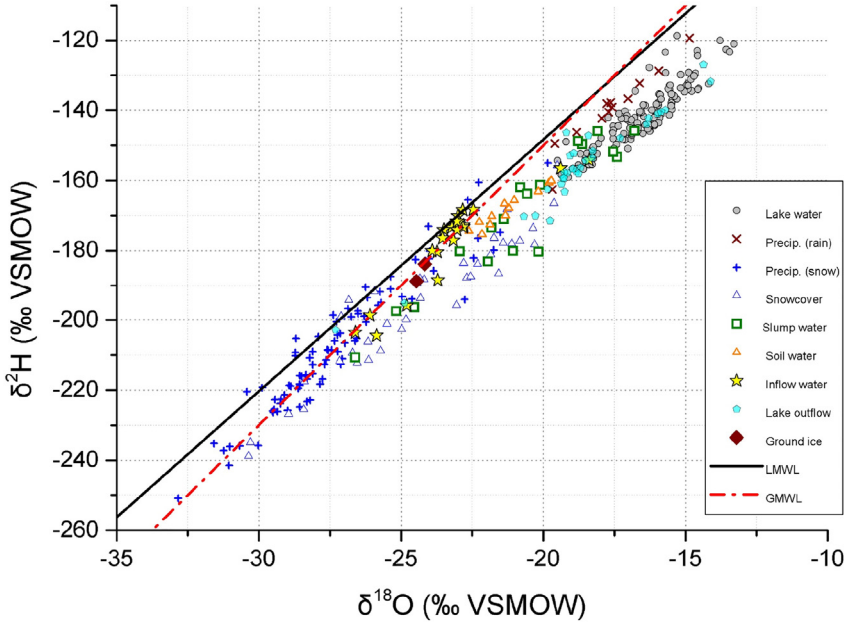

Fig. 3. Crossplot of $\delta^{18}O$–$\delta^{2}H$ showing thermokarst lake water, input sources to lakes (precipitation, snowcover, slump water, soil water, ground ice), and lake outflows. VSMOW refers to Vienna Standard Mean Ocean Water; LMWL is the Local Meteoric Water Line; GMWL is the Global Meteoric Water Line.

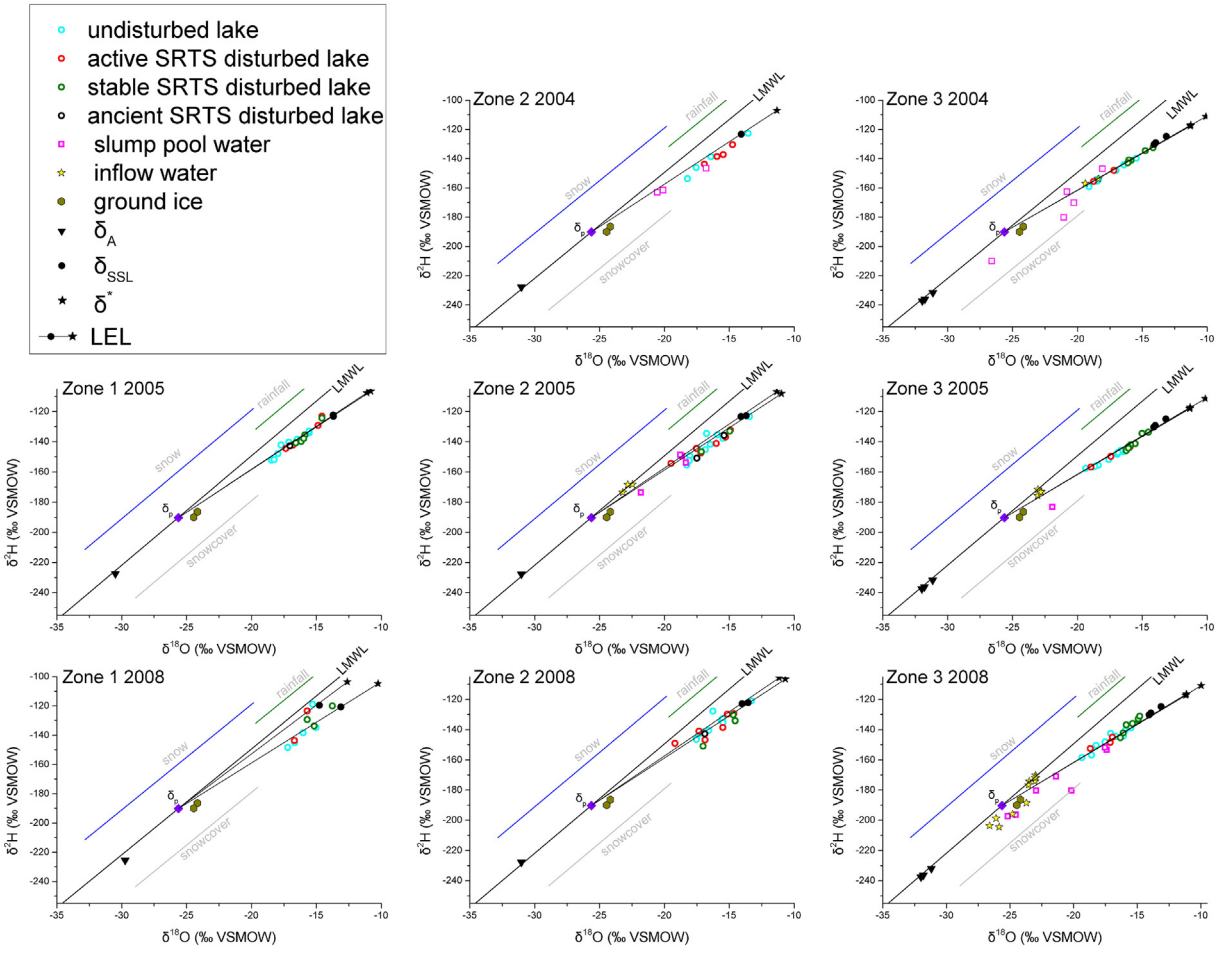

Fig. 4. The isotope framework for quantifying water balance, illustrating the relative isotopic signatures of lake water, slump water, lake inflow water and ground ice for each site. (Left panels) Zone 1: 2005 and 2008; (Centre panels) Zone 2: 2004, 2005, and 2008; (Right panels) Zone 3: 2004, 2005, and 2008.

where,

$$m = \left(h - 10^{-3}(\varepsilon_K + \varepsilon^+/\alpha^+)\right)/\left(1 - h + 10^{-3}\cdot\varepsilon_K\right) \quad (8)$$

and,

$$\delta^* = (h\delta_A + \varepsilon_K + \varepsilon^+/\alpha^+)/\left(h - 10^{-3}(\varepsilon_K - \varepsilon^+/\alpha^+)\right) \quad (9)$$

Considered that,

$$I = P + R \quad (10)$$

where P is the precipitation that falls directly on the lake surface and R is the ungauged total runoff (surface and subsurface) from the surrounding contributing area.

Therefore, R can be estimated if the evaporation amount is known:

$$R = \frac{E}{x} - P \quad (\mathrm{m}^3 \cdot \mathrm{yr}^{-1}) \quad (11)$$

where $x = E/I$, $E = e \cdot LA$ and $P = p \cdot LA$; e and p are the annual depths of evaporation and precipitation ($\mathrm{m}\cdot\mathrm{yr}^{-1}$), and LA is the lake area (m^2). Water yield (WY) can be estimated as:

$$WY = R/DBA \cdot 1000 \quad (\mathrm{mm} \cdot \mathrm{yr}^{-1}) \quad (12)$$

where DBA is the drainage basin area of individual lake (m^2). Runoff ratio is calculated as water yield divided by precipitation over the DBA. Also, the residence time of water in the lakes can be estimated as:

$$\tau = \frac{xV}{E} (\text{years} \quad (13)$$

3.4. Model parameterization

Lake areas (LA) and watershed areas (WA) were delineated from 1:30,000 scale aerial photographs and digitized to calculate their areas (Kokelj et al., 2005). Volumes (V) of 11 lakes were measured from bathymetric surveys during the sampling period. A non-linear regression line ($R^2 = 0.88$) between the measured LA and V was established to extrapolate this relationship to obtain first-approximations of V of individual study lakes. The yearly f value for each lake was estimated by using the following equation:

$$f = E{\cdot}LA/V \quad (14)$$

which reflects our basic assumption that evaporation loss was the principle driver of volumetric reduction in the lakes.

Gridded (32 × 32 km cell), monthly climate datasets from the North American Regional Reanalysis (NARR) (Mesinger et al., 2006) were used to extract annual temperature and relative humidity (both at 2 m height), as well as total precipitation and open-water total evaporation (both at ground surface) for each lake site. In the IMB model, long-term annual temperature and relative humidity (1979–2008) were processed using an evaporation-flux-weighting approach to ensure they

are representative of the evaporation season when lakes presumably underwent enrichment (see Gibson et al., 2016a). The isotopic composition of amount-weighted annual precipitation (δ_P) at Inuvik was used as an estimate of the isotopic composition of total inflow (δ_I).

As in several prior studies (e.g. Gibson et al., 2015, 2016b, 2017, 2018, 2019a), atmospheric moisture (δ_A) was initially estimated based on the assumption of isotopic equilibrium with Inuvik precipitation during the evaporation season. For representativeness of this period it was, therefore, appropriate to base the estimate on the evaporation-flux-weighted precipitation (δ_{PFW}) (Gibson et al., 2016a).

$$\delta_A = (\delta_{PFW} - \varepsilon^+)/\left(1 + 10^{-3}\varepsilon^+\right) \quad (15)$$

While this value provided a representative estimate of δ_A for inland areas, steep humidity gradients described in prior studies (Burn and Kokelj, 2009; Bigras, 1990), and confirmed by our assessment of the NARR dataset, suggest that Beaufort Sea marine vapor must also play a role in modifying the atmosphere approaching the coastline. An unscaled model without accounting for marine air mixing or seasonal volumetric drawdown was initially found to be less consistent with the observed zonal range of isotopic composition in lakes and the slope of LELs. To account for this effect, a mixing model of marine air, assumed to be in equilibrium with Beaufort Sea water, and inland moisture assumed to be consistent with Inuvik moisture, was applied to create site-specific estimates of δ_A for each lake. Proportions of each moisture source were scaled spatially in the model based on the site-specific humidity for each lake interpolated from NARR data. Zonal averages used in the model are shown in Tab1e 2. Note that Beaufort seawater near the Mackenzie Delta has been reported to be close to −4‰ for $\delta^{18}O$ (Lansard et al., 2012), so the oceanic evaporate air mass was estimated to be −17‰ in $\delta^{18}O$ under equilibrium conditions with Beaufort seawater. ^2H could then be estimated assuming it falls on the LMWL. Specifically, these adjustments corrected for a significant proportion of negative values of water yield and resulted in predicted δ^* values that were consistent with observations. Given these apparent improvements, an adjusted model accounting for marine air mixing and volumetric drawdown was used for the site-specific and zonal water balance comparisons presented in the following sections.

4. Results

4.1. Stable isotope characteristics

Stable isotope composition of rainfall, snowpack, surface runoff, and lake water, as well as select soil water and ground ice samples, are plotted in δ^2H- $\delta^{18}O$ space (Fig. 3). Precipitation values plot along the calculated Inuvik LMWL ($\delta^2H = 7.2\delta^{18}O$-4.3) with distinct distributions by precipitation type (Fig. 3). Bulk summer rainfall was found to be isotopically enriched relative to end of winter snowpack, ranging from −19.7 to −14.9‰ in $\delta^{18}O$ and −162.6 to −119.4‰ in δ^2H (Table 1). Snow surveys carried out shortly before spring freshet are shown to vary from −30.7 to −19.8‰ in $\delta^{18}O$ and −250.9 to −155.0‰ in δ^2H (Table 1). Isotopic composition of snow sampled at Inuvik during winter months is found to be within the range of snowpack values although they evidently plot along somewhat lower slopes (5.4 to 6.9) (Table 1). Ground ice collected in slump headwalls was found to be isotopically similar to shallow permafrost or retrogressive thaw flow headwalls reported in previous surveys and coring programs in the region (Lacelle et al., 2004, Lacelle et al., 2013), and is likely representative of mixed precipitation and/or runoff sources.

Lake water isotope compositions varied widely, ranging from −19.4 to −13.3‰ in $\delta^{18}O$ and from −159.1 to −118.8‰ in δ^2H, with systematic but differential enrichment occurring from the LWML along local

Table 1
Summary of stable isotopes ($\delta^{18}O$, δ^2H) for lakes, precipitation, snow cover, soil water, slump water and outflow.

Year	Zones	Lake status		$\delta^{18}O$ (‰)				δ^2H (‰)				D-excess (‰)				Regression		
			N	Min	Mean	Max	Stdev	Min	Mean	Max	Stdev	Min	Mean	Max	Stdev	Slope	Intercept	R^2
2004	Zone	Undisturbed	NA	NA	NA	NA	NA	NA	NA	NA	NA	NA	NA	NA	NA	NA	NA	NA
	1	Thaw slump	NA	NA	NA	NA	NA	NA	NA	NA	NA	NA	NA	NA	NA	NA	NA	NA
	Zone	Undisturbed	4	−18.2	−16.4	−13.6	1.8	−153.7	−140.3	−122.7	11.5	−14.2	−8.7	−5.6	3.2	6.4	−35.4	0.98
	2	Thaw slump	4	−16.9	−15.8	−14.8	0.8	−143.7	−137.4	−130.3	4.8	−13.4	−11.2	−8.3	1.9	6	−43.5	0.96
	Zone	Undisturbed	7	−19.1	−17.6	−15.5	1.2	−159.1	−150.6	−139.7	6.4	−15.9	−9.6	−6	3.6	5.1	−60.3	0.99
	3	Thaw slump	7	−18.8	−16.1	−14.2	1.4	−155.6	−142.2	−132.4	7.3	−19	−13.1	−5.4	4	5.2	−58.8	0.99
2005	Zone	Undisturbed	10	−18.5	−17	−15.6	1	−152.2	−141.9	−132.9	6.4	−9.8	−5.9	−0.3	2.7	6.1	−38.7	0.92
	1	Thaw slump	10	−17.4	−16	−14.6	1	−144.4	−136	−123	7.4	−10.5	−8.1	−5.5	1.6	7.5	−16.4	0.96
	Zone	Undisturbed	10	−18.3	−16.7	−13.5	1.4	−155.5	−142	−123.3	9.1	−15.7	−8.5	−0.4	4.2	6.1	−40.5	0.87
	2	Thaw slump	10	−19.5	−16.6	−14.9	1.4	−154.3	−142.3	−132.3	7.3	−14.5	−9.9	1.7	4.8	5	−60.1	0.92
	Zone	Undisturbed	10	−19.4	−17.9	−16.5	1	−157.7	−152.4	−145.9	4.6	−15.9	−10.4	−2.7	3.9	4.4	−73.9	0.97
	3	Thaw slump	10	−19	−16.2	−14.5	1.4	−156.7	−143.4	−133.7	7.6	−17.4	−14.1	−5	3.5	5.3	−57.2	0.96
2008	Zone	Undisturbed	5	−17.2	−16	−15	0.8	−148.3	−137	−118.8	10.3	−14.4	−8.7	3.6	6.3	10.3	27.5	0.66
	1	Thaw slump	5	−16.7	−15.4	−13.8	1	−143.6	−130	−120.1	8.2	−12.3	−6.7	2.2	5.3	6.7	−26.1	0.61
	Zone	Undisturbed	10	−17.6	−16.2	−13.3	1.2	−146.4	−136.7	−121	7.7	−14.6	−7	2.4	4.3	5.7	−44.8	0.83
	2	Thaw slump	10	−19.2	−16.2	−14.6	1.4	−150.9	−139.2	−129.5	7.7	−17.6	−9.7	4.6	6.3	4.6	−64.7	0.74
	Zone	Undisturbed	10	−18.6	−17.1	−15.5	1.1	−156.8	−146.3	−138.7	5.5	−15.5	−8.9	−3.6	4.2	4.8	−64.7	0.86
	3	Thaw slump	10	−17.1	−15.8	−14.8	0.8	−148.4	−139.1	−131.2	5.9	−14.8	−11.6	−2.9	3.4	6.9	−30.6	0.93
		Rainfall	12	−19.7	−17.6	−14.9	1.3	−162.6	−139.4	−119.4	10.3	−5.1	1.3	7.3	3	7.4	−9.8	0.92
2008	Zone	Coastal fen snow	14	−32.8	−28.4	−25.7	1.7	−250.9	−217.2	−195	13.5	5.2	10	12.7	2.3	7.8	−9.6	0.97
	3	Transit area snow	16	−30.7	−27.1	−21.5	2.3	−235.9	−206	−168.6	17.1	−2.6	11.1	20.6	5.8	7	−15.7	0.9
		Interior plateau snow	54	−31.6	−26.8	−19.8	2.6	−241.5	−204.2	−155	19.6	−12	10.5	20.5	6.6	7.1	−12.5	0.9
		Snow in slumps	3	−30.4	−29.5	−28.9	0.6	−223.8	−221	−218.7	2.1	10.2	15.3	22.9	5.5	NA	NA	NA
		Coastal fen snow on ice	12	−28.4	−22.4	−19.6	2.6	−225.5	−184.3	−166.5	16.4	−15.8	−5	5.2	7.1	6	−49.4	0.91
		Transit area snow on ice	8	−29	−23.8	−19.5	3.1	−226.8	−192.2	−155.7	21.6	−6.5	−1.7	5.5	4.7	6.9	−28	0.98
		Interior plateau snow on ice	9	−28.4	−24.9	−22.6	1.6	−217.6	−200.6	−187.5	9.9	−11.4	−1.2	9.6	6	5.4	−65.2	0.81
		5A soil water	6	−22.2	−21	−19.7	0.9	−175.4	−167	−160.1	5.7	−2.3	0.7	2.6	2.1	6	−41.5	0.97
		5B soil water	6	−22.6	−21.6	−20.2	0.8	−174.4	−169.4	−163.1	3.6	−1.7	3.4	6.4	2.9	4.5	−73	0.91
		Slump water	19	−26.6	−20.8	−16.8	2.9	−209.9	−169.8	−146.5	3.9	−18.9	−3.8	4	4.9	6.7	−29.47	0.9
		Lake inflow water	22	−26.6	−23.2	−18.4	1.8	−204.4	−177.7	−153.8	12.9	−6.7	8.7	14.2	5.2	6.8	−20.5	0.87
		Lake outflow water	31	−27.3	−18.8	−14.1	2.9	−202.9	−157	−127	3.9	−18.8	−5.9	15.5	4.9	6	−44.5	0.95
		Ground ice	2	−24.4	−24.3	−24.2	0.1	−190.2	−187.9	−185.6	2.3	5.1	6.3	7.6	1.3	NA	NA	NA

evaporation lines (LEL; Fig. 4). This is consistent with lakes spanning a diverse range of water balance conditions (MacDonald et al., 2016). SRTS affected lakes were found to have mean values of −16.1 and −139.7‰ for $\delta^{18}O$ and $\delta^{2}H$, respectively, ranging from −19.5 to −13.8‰ for $\delta^{18}O$ and −156.7 to −120.0‰ for $\delta^{2}H$. This was not significantly different on average than undisturbed lakes, which had mean values of −16.9 and − 143.8‰ for $\delta^{18}O$ and $\delta^{2}H$, respectively, ranging from −19.4 to −13.8‰ for $\delta^{18}O$ and − 156.7 to −120.1‰ for $\delta^{2}H$. Several undisturbed lakes plotted close to the LMWL, and evidently were isotopically similar to rainfall. Undisturbed lakes plotted along a steeper LEL than SRTS lakes (6.3 vs. 5.7), possibly influenced by greater snowmelt runoff contributions to the latter.

Overall, there were only subtle divergences between the isotopic composition of lake waters and corresponding outflows (±0.8‰), suggesting that lakes were generally well mixed in the late open-water season at the time of sampling. Isotopically, lake inflows were more similar to snowpack and ground ice than rainfall (Table 1), indicating snowmelt, and/or permafrost meltwater, dominated the near surface runoff. Similarly, soil waters spanned a narrow range of isotopic values (−22.6 to −17.9‰ for $\delta^{18}O$ and −175.4 to −160.1‰ for $\delta^{2}H$), appearing to be a mixture of snow and rainfall with minor evaporative enrichment. Variable isotope compositions were noted for slump runoff pools, which ranged from −30.4 to −16.3‰ for $\delta^{18}O$ and −223.8 to −142.3‰ for $\delta^{2}H$, with evaporative isotopic imprints. Regression of slump runoff and pool samples yielded an LEL defined by $\delta^{2}H = 6.7\ \delta^{18}O$ - 29.5, with values that significantly overlap with snowpack, rainfall, ground ice, and surface runoff.

4.2. Isotope framework validation

Measured and modeled isotopic parameters were used to define an isotope balance framework for each sampling year and climate zone (Table 2 & Fig. 4). The isotopic signature of inflow to lakes (δ_I), falling close to the LMWL, was approximated in the model for all zones as the isotopic composition of mean annual precipitation (δ_P) calculated from GNIP data to be −25.6‰ for $\delta^{18}O$ and −190.1‰ for $\delta^{2}H$. Zone-specific, year-specific LELs, capturing differences in evaporation controls for water bodies with range of evaporation/inflow conditions, were then calculated and compared to observations (Table 1 & Fig. 4). LELs were found to be steeper in Zone 1, ranging from 5.5 to 6.7, shallower in Zone 3, ranging from 5.0 to 5.1, and intermediate for Zone 2, ranging from 5.6 to 5.8. Variations in LEL slopes were ably replicated by the model scenarios, and as such are attributed to a balance between marine and continental climate influences. Overall, spatial variations in the LEL slopes across the region were found to be systematic and broadly consistent with regional observations (Gibson and Edwards, 2002; Gibson et al., 2016a), and global predictions (Gibson et al., 2008).

4.3. Lake water balance calculations

Site-specific ratios of evaporation/inflow (E/I), precipitation/inflow (P/I), water yield (WY), runoff ratio (R/P), and residence time (τ), were determined for individual lakes (Fig. 5 & Table 3). Note that P/I was estimated using precipitation on the lake surface in order to emphasize partitioning of precipitation versus water yield to the lake. For the catchment water balance assessment, the most relevant indicator is the R/P, which reflects partitioning of runoff as compared to evaporation or storage changes. Note that corrections for seasonal volumetric reduction based on Eq. (6) were applied to all lakes and years based on site-specific characteristics. Implementation of this correction, which effectively resulted in slight reduction (5–10%) in estimated values for E/I and an increase in estimated WY compared to an uncorrected model, is considered in the present setting to be more representative of long-term steady-state water balance for all lakes. It also eliminated spurious negative water yields for nearly all lakes. Several exceptions were found where this simple correction was ineffective, evidently due to more extreme drying conditions or the effect of taliks contributing to enhanced lake losses, as discussed later on.

Based on three years of observations, undisturbed lakes were found to have low E/I ratios relative to disturbed lakes, ranging from 0.09 to 1.19, with an average value of 0.38 (Fig. 5). Over three-quarters of undisturbed lakes were found to lose less than half of their inflow via evaporation. Ancient SRTS lakes show similar water balance conditions ($E/I < 0.4$), although only three were investigated. E/I ratios were slightly higher among active SRTS lakes, varying from 0.08 to 0.84 with an average value of 0.46, suggesting positive water balances. Stable SRTS lakes had significantly greater E/I ratios, averaging 0.67 with a range spanning between 0.17 and 1.38. 13 of 16 lakes in this category were evaporation-dominated lakes ($E/I > 0.5$) based on the classification of Turner et al. (2010). Based on P/I, direct precipitation falling onto lake surfaces accounted for over 40% of inflows for over half the lakes, and as such was an important water source. This was found to be especially true for evaporation-dominated lakes ($E/I > 0.5$), where mean P/I was as high as 0.79, and only two lakes in this subgroup were below 0.5, indicating that runoff sources from these catchments may be less dynamic, perhaps limiting lake throughflow and enhancing the proportion of water loss to evaporation.

Mean annual water yields were found to be highly variable, ranging from near zero to as high as 600 mm across the study region (Fig. 5). Water yields of undisturbed lakes ranged up to 475 mm with an average of 88 mm. Although water yields of active SRTS lakes had narrow ranges (up to 156 mm), they shared very similar mean value of 71 mm with undisturbed lakes, while lower water yields were found in stable SRTS lakes, averaging 54 mm and reaching high values of 336 mm. Although the average water yields for undisturbed lakes and active SRTS lakes were similar (within 20 mm), active SRTS lakes were found to have slightly higher water yields, whereas stable SRTS lakes often had lower water yields than undisturbed lakes.

Negative water yields, i.e. ranging from −40 to −10 mm, are predicted for five evaporation-dominated lakes (Fig. 5). As seasonal evaporative drawdown was already accounted for using Eq. (6), such outputs are attributed to extreme E/I indicative in many cases of long-term volumetric drawdown (e.g. Lake 8a: 1.19; Lake 2b: 1.07; Lake 26b: 0.83; Lake 30b: 1.38), or highly evaporative long-term water balance (Lake

Table 2
Measured and calculated parameters used within the isotopic framework to quantify water balances.

Parameter	Zone 1		Zone 2			Zone 3		
	2005	2008	2004	2005	2008	2004	2005	2008
FW T (K)	272.8	271.6	274.4	274.7	274.6	278.7	278.4	278.7
FW h	0.79	0.81	0.75	0.75	0.75	0.72	0.72	0.71
α^{+} (^{18}O, ^{2}H)	1.0119, 1.1126	1.0120, 1.1146	1.0116, 1.1098	1.0116, 1.1093	1.0117, 1.1096	1.0112, 1.1033	1.0112, 1.1037	1.0112, 1.1033
ε^{+} (^{18}O, ^{2}H)	0.119, 0.113	0.012, 0.115	0.0116, 0.109	0.012, 0.110	0.012, 0.110	0.0112, 0.103	0.0112, 0.104	0.0112, 0.103
ε_K (^{18}O, ^{2}H)	3.23, 2.85	3.11, 2.74	3.49, 3.07	3.51, 3.09	3.54, 3.11	4.01, 3.52	3.98, 3.51	4.06, 3.57
δp (^{18}O, ^{2}H) ‰	−25.6, −187.5	−25.6, −187.5	25.6, −187.5	25.6, −187.5	25.6, −187.5	25.6, −187.5	25.6, −187.5	−25.6, −187.12
δ_A (^{18}O, ^{2}H) ‰	−30.5, −227.4	−29.7, −225.5	−31.0, −227.7	−31.0, −227.7	−30.9, −227.1	−32.0, −235.0	−31.8, −235.9	−31.7, −235.5
δ_{SSL} (^{18}O, ^{2}H) ‰	−14.3, −122.1	−13.9, −120.1	−15.0, −132.2	−13.9, −123.1	−13.8, −122.5	−13.7, −128.0	−13.8, −128.2	−13.7, −124.8
δ^{*} (^{18}O, ^{2}H) ‰	−11.7, −106.4	−11.4, −104.1	−12.6, −119.1	−11.2, −107.5	−10.9, −106.1	−10.9, −115.3	−10.9, −115.5	−10.8, −114.9

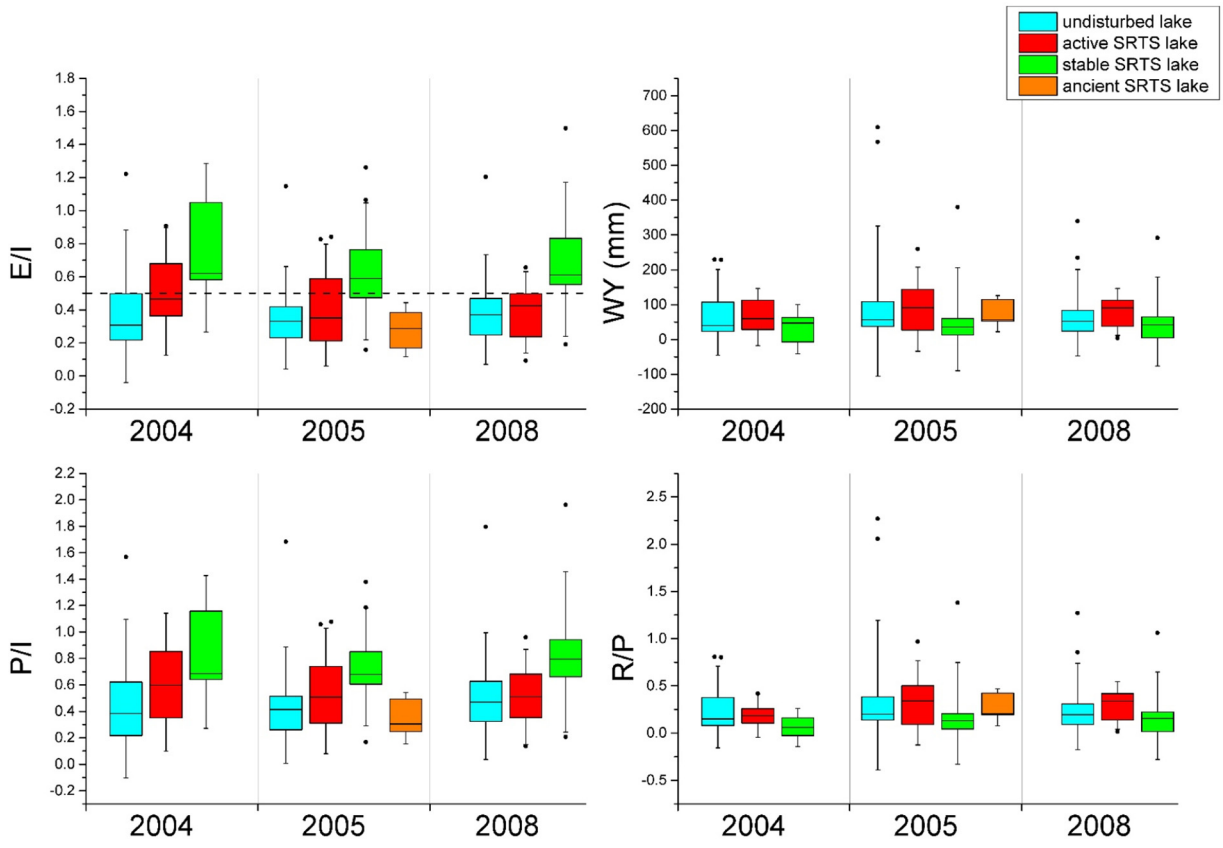

Fig. 5. Box plots showing the derived isotope mass balance indicators, namely E/I, P/I, water yield (WY), and runoff ratios (R/P), in three study years.

34b: 0.84). Negative water yields are a clear indication that the simple IMB model may not be valid for such lakes. We presume that this reflects additional unaccounted for water losses, as may be expected in the case of lakes recharging unfrozen taliks, or possibly due to underestimation of lake areas at these sites.

Extremely high water yields, in the range of 1.27 to 2.27 times the depth of precipitation falling on the catchment, were also found in some undisturbed lakes as well as stable SRTS lakes (Lakes 16a, 19a, and 19b) (Fig. 5). The undisturbed lakes showed larger variability in R/P as compared to other lake types, but more than half of these lakes had low runoff ratios below 0.2 (Table. 3). Higher runoff ratios were found in active SRTS lakes, varying from 0 to 0.42. Runoff ratios in these systems averaged 0.19 in 2004, but tended to be higher both in 2005 and 2008, averaging close to 0.3 in both years. Stable SRTS lakes also exhibited low runoff ratios (0 to 0.41), with the exception of Lake 19b.

Estimated residence time for individual lakes ranged from 1.1 to 51.4 years, with an average of 9 years for undisturbed lakes, 12.2 years for active SRTS lakes, 15 years for stable SRTS lakes, and 5.1 years for ancient lakes (Fig. 5). With the exception of ancient lakes, these differences suggest that slumping processes may contribute to a decrease in the rapidity of water flushing in each watershed, and might similarly impact the regional runoff. Overall, validity of the IMB approach based on long-term climate data, long-term isotope data for precipitation, and lake water isotopic records is further supported by the finding of multi-year residence times for all lakes.

4.4. Sensitivity analysis

A sensitivity analysis was conducted to test the reliability of the IMB model outputs by varying controlling input parameters by up to 5% including T, RH, δ_A, and f. A similar approach was used by Gibson et al. (1993) to illustrate sensitivity of a steady-state isotope balance model for two sites in northern Canada. Due to non-linearity, examples are used to illustrate the sensitivity of E/I, P/I, WY, and R/P for two lakes with contrasting isotopic enrichment (Table S4). One lake is a high throughflow lake, plotting with minor offset along the LEL (Lake 5b) and a second is an evaporation-dominated lake, plotting significantly offset along the LEL (Lake 8a). We found that temperature (T) has a negligible impact on E/I ratios (<1%) for both lakes, whereas uncertainty in RH and δ_A may potentially lead to significant differences in the IMB outputs. A similar degree of sensitivity was found for P/I, WY, and R/P (Table S4). Evaporation-dominated lakes are shown to be more sensitive to RH and δ_A than high throughflow lakes where uncertainties appear to be restricted to <10%. In contrast, model sensitivity to values of f appear to be accentuated in high throughflow lakes as compared to

Table 3
Summary of three-year averages of water balance indicators by lake type.

	Residence time (yr)		E/I		P/I		Wy (mm)		R/P	
	Mean ± SD	Median	Mean ± SD	Median	Mean ± SD	Median	Mean ± SD	Median	Mean ± SD	Median
Undisturbed lake	9.0 ± 4.6	7.0	0.38 ± 0.22	0.37	0.48 ± 0.21	0.42	88 ± 100	53	0.32 ± 0.34	0.19
Active SRTS lake	12.2 ± 5.8	9.3	0.46 ± 0.26	0.42	0.59 ± 0.24	0.55	71 ± 72	80	0.25 ± 23	0.30
Stable SRTS lake	15.0 ± 6.3	11.5	0.67 ± 0.30	0.59	0.79 ± 0.26	0.72	54 ± 88	37	0.19 ± 0.22	0.14
Ancient SRTS lake	5.1 ± 2.6	3.2	0.29 ± 0.07	0.29	0.37 ± 0.05	0.31	67 ± 22	56	0.25 ± 0.09	0.20

evaporation-dominated lakes, although high throughflow lakes usually tend to be maintained at near constant volume due to the fill and spill mechanism. Based on significant but differential sensitivity of the model, as identified in this analysis, it becomes apparent that use of site-specific climate information is essential to best account for regional variability, as we do by applying the NARR climatology. We also suggest that site-specific quantitative interpretation be interpreted with some caution, most appropriately in the context of a comparative lake-to-lake assessment rather than as a standalone analysis for a single watershed.

5. Discussion

Our analysis provides new site-specific evidence of water balance variations in response to climate, permafrost conditions, and wildfire across the study region based on a comprehensive set of IMB indicators (E/I, P/I, WY and R/P). While previous studies such as Leng and Anderson (2003), Anderson et al. (2013), MacDonald et al. (2016) and Narancic et al. (2017) also employed IMB to estimate E/I from numerous lakes in thermokarst terrain, they did not attempt to determine WY or R/P, and as a result reported variability related mainly to lake water budgets rather than catchment-weighted effects of permafrost degradation on runoff generation processes. Effectiveness of our comprehensive approach using both lake indicators (E/I, P/I) and watershed indicators (WY and R/P) was also recently demonstrated in characterizing hydrologic variations across permafrost thaw trajectories in the Yellow River headwaters (Wan et al., 2019), and in northern Alberta (Gibson et al., 2015, 2019b). Fortunately, transformation of IMB results to obtain the landscape indicators is relatively straightforward, requiring only estimates of lake and watershed areas, which can be routinely estimated from a spatial delineation analysis. A typical approach has been described in Gibson et al., (2010). Our assertion is that there may be considerable incentive to revisit collection of basic watershed information for some of the isotopic surveys conducted in the past, including many carried out in remote areas and/or in permafrost terrain.

5.1. Coastal-inland climate and water balance gradients

In the following we provide a description and illustration of systematic hydrologic responses from several perspectives, including box plots comparing statistical differences between lake types (Figs. 5, 7), and a transect perspective intended to enhance visibility of spatial variability including any noise in the dataset (Fig. 6). It is anticipated that these complimentary perspectives offer more complete insight into complex hydrologic responses of lakes and watersheds in the region.

From near shore (Zone 1) extending to inland sites (Zone 2), a progressive decrease in E/I and P/I is evident (Fig. 6), with relaxation or complete reversal in these trends for inland areas dominated by ancient thaw lakes (Zone 3). Along the same transect, WY and R/P were found to respond inversely to E/I and P/I, increasing steadily from near shore (Zone 1) to inland sites (Zone 2), with lower values being associated with ancient thaw lake terrain (Zone 3). Concurrence of high values of E/I and P/I for coastal areas is likely indicative of a higher degree of lake closure and a reduced role of runoff replenishment to lakes in this

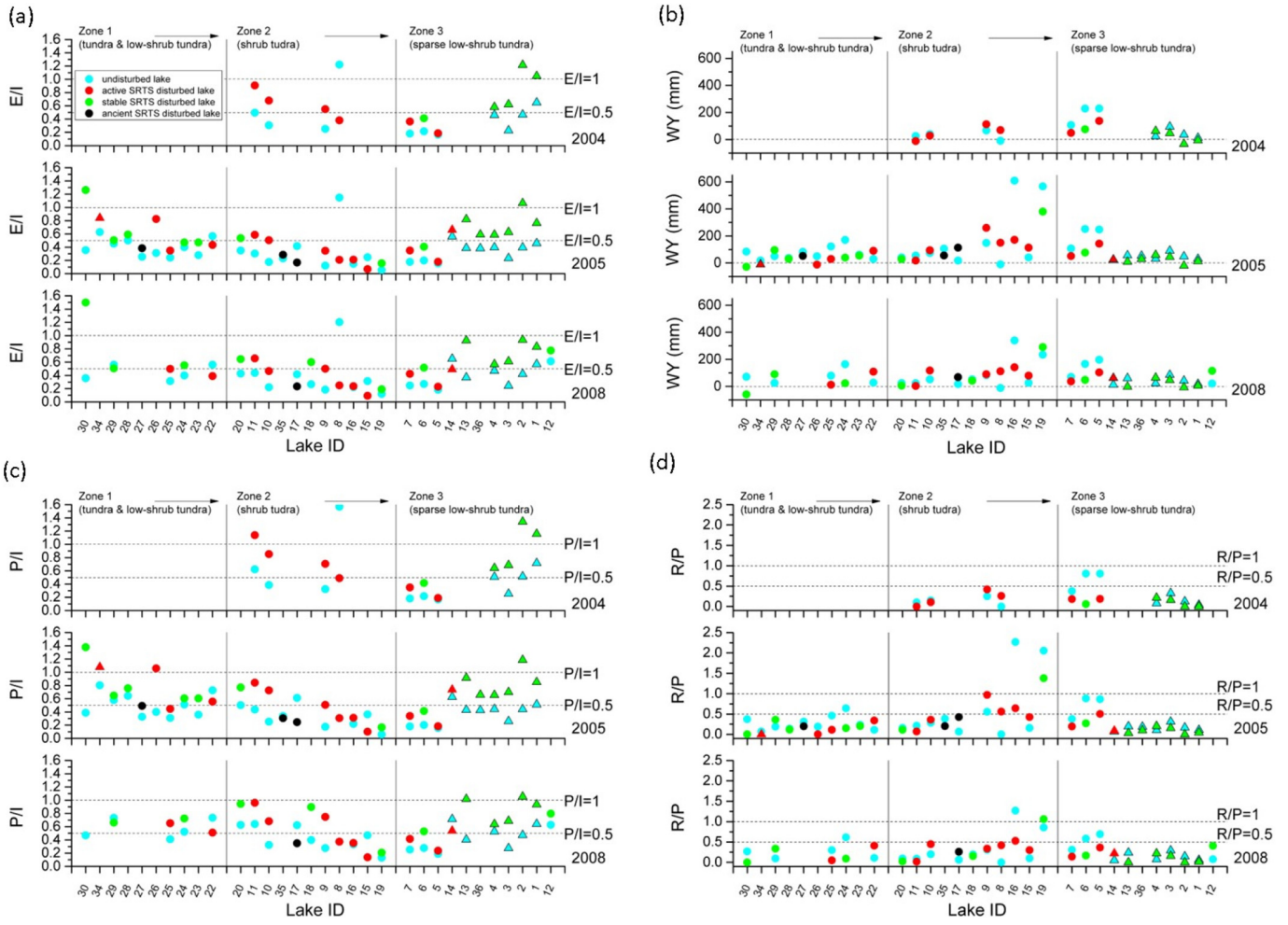

Fig. 6. Zonal summary of calculated water balance indicators, (a) E/I (b) WY, (c) P/I, and (d) R/P. For each indicator, data are shown by year (stacked vertically) and by zone (side-by-side) for 2004, 2005, and 2008. Triangles (▲) indicate lakes with recent burn history; circles (●) indicate no recent burn history. Lake types are further differentiated by colour (see legend).

area. Conversely, concurrence of low E/I and P/I at inland sites reveals greater influence from runoff, which is also indicated by higher WY and R/P in these areas. Large zonal gradients are thus apparent from evaluation of site-specific water balance results across the network, reflecting pronounced climate and vegetation gradients on the landscape and the overriding effect of permafrost degradation due to both long-term climate change and recent wildfire.

While systematic differences are noted among the different lake disturbance categories across the various zones, all lakes appear to follow the same general regional pattern described above (Fig. 6). It is also important to note that individual lakes sampled in multiple years were found to yield comparable IMB outputs and zonal patterns from year to year, although the values also appeared to respond to interannual climate variability.

Based on the NARR dataset, important trends defining the coastal-inland climate gradient and controlling the overall variations in hydrologic setting included: (i) decrease in relative humidity, (ii) increase in air temperature, (iii) increase in precipitation, (iv) increase in evaporation, and (v) decrease in P-E (Fig. S1). Ground temperatures have also been measured and shown to increase from coastal areas with low shrub tundra (Zone 1) to inland areas (Zone 2) (see Burn and Kokelj, 2009), which is expected to influence active layer development, permafrost degradation, and thereby runoff generation. Variations in WY were also expected spatially and interannually in response to melting of variable snowcover, which is known to accumulate preferentially in areas with better developed shrub tundra such as Zone 2, or in association with depressions including lakes and thaw slumps. The potential effect of snowmelt on runoff is apparent from decline in average WY in 2008 for Zone 2 by 62 mm (~41%) compared to 2005 due to lighter snow cover in the latter year. Antecedent moisture conditions might also have played a role, as 2007 had anomalously low precipitation that might have limited soil moisture content prior to the 2008 thaw season.

It should be noted that Zone 3 is an area with documented recent wildfire impacts with the exception of lake sites 5, 6, and 7, located near the transition between Zones 2 and 3, that were recognized to have had no recent burn activity. As a result, these unburnt lakes displayed hydrological conditions typical of Zone 2. For lakes in Zone 3, situated in watersheds affected by the 1968 wildfire (7 lakes), a common water balance impact appeared to be systematically elevated E/I and P/I, but with extremely low WY (35 mm on average) and low R/P. This appears to be the general case for lakes affected by wildfire across the network (Fig. 7).

Key drivers that explain the hydrological differences among lakes with/without burn history are likely associated with permafrost degradation. Intense wildfire is expected to reduce vegetation cover and near surface organic materials, leading to acceleration of active-layer deepening and thawing of near surface-permafrost. Although dense alder and willow shrubs are typically reestablished in burn areas (Landha¨usser and Wein, 1993), significantly lower water yields and runoff ratios observed among every lake category (ANOVA, $p < 0.001$) indicates weaker runoff generation capacity here as compared to other catchments with shrub tundra vegetation (Table S2).

5.2. Permafrost degradation and disturbances including SRTS

Regional permafrost degradation has been examined across the study area through mapping of SRTS frequency and watershed areal extent (Houben et al., 2016), as well as monitoring of near-surface ground temperature (Burn and Kokelj, 2009; Kokelj et al., 2017). These studies were effective at establishing the role of slumping in alteration of

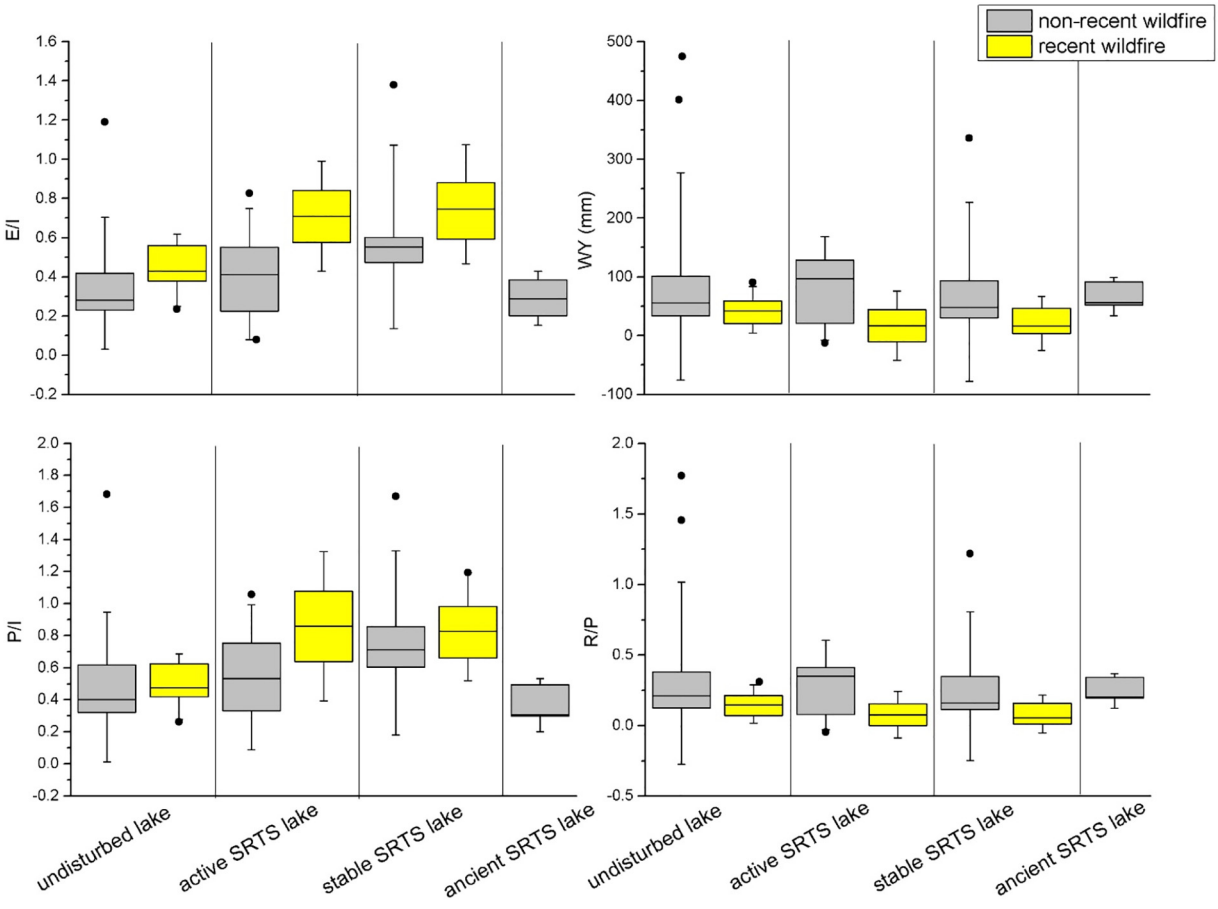

Fig. 7. Systematic differences apparent in water balance indicators for lakes influenced by recent wildfire. Indicators include: (a) E/I, (b) WY, (c) P/I, and (d) R/P.

biogeochemical cycles in area lakes. SRTS is the most obvious permafrost degradation feature across the region, with various generations of occurrences including active, stable, and ancient varieties. Relatively little information has previously been published comparing water balance of various slump lake types or comparing slump lakes with undisturbed systems. Our isotope-based comparisons reveal extremely systematic patterns among lake categories, strongly indicating that slumping leads to increase in proportion of evaporative losses from lakes (i.e. increased E/I), increase in replenishment of the lakes by direct precipitation (i.e. increased P/I), and short-term increases and eventual decline in WY and R/P from the landscape (Fig. 5).

Previous hydrologic studies across continuous/discontinuous permafrost thaw trajectories in Qinghai-Tibet (Wan et al., 2019) and northeastern Alberta (Gibson et al., 2015, 2019b) have shown a strong relationship between water yield (and runoff ratio) and permafrost extent in the watershed. Conceptually, both studies have ascertained that permafrost degradation generated a pulse of runoff similar to an event hydrograph, with peak thaw-related runoff occurring once significant taliks form, but while permafrost still covers a significant proportion of the land area. Eventually, reduction in permafrost extent effectively leads to recession in thaw-related runoff. In defining a similar permafrost thaw trajectory in the present study, a comparable response might be depicted by the various stages of slumping, but we also propose that the thaw trajectory might also manifest an analogous cycle on the regional scale. It is informative to note that WY is generally found to be lower in coastal areas with colder ground temperatures and thicker, colder permafrost (Zone 1), and increases to its highest levels moving to inland areas with warmer ground temperatures and warmer permafrost (Zone 2). Conceptually, we suggest this regional gradient in WY potentially reflects progressive stages of thaw intensity along the rising limb of the permafrost thaw hydrograph. In this case, sites with a higher degree of permafrost degradation and greater thawing are generate greater runoff than sites at an earlier stage of thawing. As for Zone 3, two main clues suggest that the permafrost degradation cycle has already peaked in these watersheds, as both ancient thaw lakes and recent wildfire affected sites are known to have a history of permafrost thaw and are now characterized by below average WY and R/P. This is a testable hypothesis, as it generally implies that thaw-generated runoff is likely to increase in Zone 1 and decrease in Zone 2 over time, whereas for Zone 3 it is likely to remain more stable over time into the future.

5.3. Physical and hydrological evolution of slump lakes

Compared to undisturbed lakes, active SRTS lakes have higher WY. This process is clearly reflective of permafrost degradation and is presumably linked to degree of impact, as a positive relationship was found between WY and thaw slump area/lake area ratios ($R^2 = 0.46$, $p < 0.012$). The statistically significant positive correlation between lake area, catchment area, and active thaw slump area implies that the growth of active SRTS promotes the lateral expansion of thermokarst lakes. These lakes are typically deeper than undisturbed lakes, where lake bottom taliks might form that potentially support new hydrological flowpaths, leading to longer residence times of runoff (Vonk et al., 2015). Increased interaction between subsurface flow and lake water resulting from permafrost degradation appear to enhance the effect of evaporation, as E/I was found to be higher for active SRTS lakes than for undisturbed lakes, although water balances were still in positive status. High E/I ratios were also found for larger surface area lakes, reflecting decreased inflows from the watershed as thermokarst lakes developed and matured.

Later, as continued development of SRTS enters into the stable phase (see Houben et al., 2016), the capacity of landscape water production is expected to dramatically decline due to the gradual disappearance of previously frozen water sources. WY appears to decline in the stable phase (Fig. 5). Note that stable SRTS lakes typically had smaller CA/LA ratios, ranging from 1.6 to 6.3, compared to active SRTS lakes, which averaged 6.6. Evolution by expansion of thermokarst lake area appears to have accompanied the permafrost degradation process, and growth of lakes at the expense of the surrounding drainage basin has served to reinforce reduction in landscape runoff and concomitant reduction in lake throughflow. At this stage, it can be concluded that SRTS near lake shorelines or in catchments induces more negative water balances in thermokarst lakes, as gradual reduction in permafrost thaw sources as well as decreasing water storage on the landscape no longer offset evaporation from the lake, and the lakes therefore tend towards evaporation-dominated status (Connon et al., 2014). We suggest that multiple generations of thaw lakes may have arisen from activation or reactivation of the SRTS process with climate change, presumably since the Little Ice Age. Overall, we find robust but complex hydrological responses of both lakes and landscapes to permafrost degradation and slumping based on stable isotope characteristics of the small watersheds.

6. Summary and conclusions

Based on a paired-lake water sampling program carried out in 2004, 2005 and 2008 including 64 upland lakes adjacent to the Mackenzie Delta Region, we applied water isotopic signatures of multiple source waters, surface waters, and soil waters to estimate water balance parameters for lakes and watersheds using a novel, steady-state IMB approach incorporating corrections for seasonal evaporative drawdown in lakes and marine-continental air mixing. Site-specific hydrologic indicators, including E/I, P/I, WY and R/P were used to create a robust perspective of lake and watershed hydrologic conditions across a coastal-inland transect, and among various types of lakes with evidence of differential permafrost degradation including slumping. Results suggest distinct spatial patterns in site-specific hydrological conditions from Zone 1 to Zone 3 controlled largely by climate, vegetation and permafrost degradation gradients, but dependent also on site-specific catchment characteristics and year-to-year meteorological conditions during the thaw season. Spatially, lake water balance tends towards more positive status (decreasing E/I ratios) along a clear hydrological trajectory from the near-coastal to inner uplands (NW-SE transection). The isotope framework interpreted using IMB also suggested significantly higher WY and R/P in watersheds where dense shrubs effectively led to higher snowcatch and snowmelt runoff, while significantly lower runoff was determined for watersheds where vegetation and organic matter has largely been removed or reduced by recent wildfire. We suggest that snowmelt dominated lakes may be the most vulnerable to future climate changes and specifically wildfire.

A robust temporal evolution of hydrological impacts related to permafrost thaw is proposed based on our observations in the Mackenzie Delta region and in analogous cold regions systems undergoing permafrost degradation including discontinuous permafrost regions of northern Alberta and Tibet. As active slumps are established and continue to grow, they appear to release water stored in both the slump areas and within ice–rich permafrost in the catchment, which combines to increase runoff and promote lake expansion. Later, when the development of thaw slumping stabilizes, the gradual disappearance of previously frozen water sources leads to reduction in runoff, and negative water balances emerge, with a trend towards evaporation-dominated conditions and possibly lake shrinkage. Thermokarst activity and associated land-cover changes driven by permafrost thaw appear to control catchment runoff and connectivity, which influenced regulation of rainfall, snowmelt runoff and additional local subsurface flows.

Further research is recommended to examine similar responses to permafrost thaw at a wider network of sites, including coupling water quality sampling with such assessments to address water quantity-water quality relationships, greenhouse gas regulation, and additional biogeochemical impacts. This will expectedly contribute to better

understanding of linkages between water and carbon cycle impacts related to increasingly widespread reports of permafrost degradation.

CRediT authorship contribution statement

Chengwei Wan: Conceptualization, Data curation, Methodology, Formal analysis, Visualization, Writing - original draft.**John J. Gibson:** Conceptualization, Methodology, Validation, Funding acquisition, Writing - review & editing.**Daniel L. Peters:**Conceptualization, Investigation, Project administration, Resources, Funding acquisition, Writing - review & editing.

Declaration of competing interest

We wish to confirm that there are no known conflicts of interest associated with this publication and there has been no financial support for this work that could have influenced its outcome.

We confirm that the manuscript has been read and approved by all named authors and that there are no other persons who satisfied the criteria for authorship but are not listed. We further confirm that the order of authors listed in the manuscript has been approved by all of us.

We confirm that we have given due consideration to the protection of intellectual property associated with this work and that there are no impediments to publication, including the timing of publication, with respect to intellectual property. In so doing we confirm that we have followed the regulations of our institutions concerning intellectual property.

We understand that the Corresponding Author is the sole contact for the Editorial process (including Editorial Manager and direct communications with the office). He is responsible for communicating with the other authors about progress, submissions of revisions and final approval of proofs. We confirm that we have provided a current, correct email address which is accessible by the Corresponding Author.

Acknowledgements

We thank those who facilitated the upland lakes study program and supported collection of isotope samples including Steve Kokelj, Government of Northwest Territories and scientists from Environment and Climate Change Canada (ECCC), including Terry Prowse (Emeritus Scientist), Fred Wrona (currently with Alberta Environment and Parks), and Tom Carter. We also thank Jean-Francois Helie, GEOTOP, Universite du Quebec a Montreal, for co-designing the isotopic investigations carried out in 2004 and carried forward by Daniel Peters. We thank Zhou Zhou (Nanjing, China) for assisting with graphical abstract design, and CW thanks Zhou Zhou for advice on an early draft. University of Victoria graduate students, Megan Thompson and Patricia Mesquita, are acknowledged for field assistance including sample collection. Funding for this research was obtained from Environment and Climate Change Canada, Polar Continental Shelf Program, International Polar Year, Natural Sciences and Engineering Research Council of Canada, and InnoTech Alberta. Fieldwork for this project was carried out under research permits issued by the Government of Northwest Territories administered by the Aurora Research Institute. Chengwei Wan received support to participate in data interpretation from InnoTech Alberta, University of Victoria, the Key Program of National Natural Science Foundation of China (Grant No.51539003), the National Natural Science Foundation of China (Grant No. 51979072) and the Strategic Priority Research Program of Chinese Academy of Sciences (XDA2010010307) from Prof. Zhongbo Yu and Prof. Peng Yi.

Appendix A. Supplementary data

Supplementary data to this article can be found online at https://doi.org/10.1016/j.scitotenv.2020.139176.

References

Abbott, B.W., Larouche, J.R., Jones Jr., J.B., Bowden, W.B., Balser, A.W., 2014. Elevated dissolved organic carbon biodegradability from thawing and collapsing permafrost. J. Geophys.Res. Biogeosciences. 119 (10), 2049–2063.

Abbott, B.W., Jones, J.B., Godsey, S.E., Larouche, J.R., Bowden, W.B., 2015. Patterns and persistence of hydrologic carbon and nutrient export from collapsing upland permafrost. Biogeosciences 12 (12), 3725–3740.

Anderson, L., Birks, J., Rover, J., Guldager, N., 2013. Controls on recent Alaskan lake changes identified from water isotopes and remote sensing. Geophys. Res. Lett. 40 (13), 3413–3418.

Arp, C.D., Jones, B.M., Liljehahl, A.K., Hinkel, K.M., Welker, J.A., 2015. Depth, ice thickness, and ice-out timing cause divergent hydrologic responses among Arctic lakes. Water Resour. Res. https://doi.org/10.1002/2015WR017362.

Balser, A.W., Jones, J.B., Gens, R., 2014. Timing of retrogressive thaw slump initiation in the Noatak Basin, northwest Alaska, USA. J. Geophys.Res.: Earth Surface 119 (5), 1106–1120.

Bigras, S., 1990. Hydrological Regime of Lakes in the Mackenzie Delta, Northwest Territories, Canada. Arctic Alpine Res 22 (2), 163–174. https://doi.org/10.1080/00040851.1990.12002778.

Birks, S.J., Gibson, J.J., Gourcy, L., Aggarwal, P.K., Edwards, T.W.D., 2002. Maps and animations offer new opportunities for studying the global water cycle. Eos, Trans. Amer. Geophys. Union 83 (37), 406.

Bouchard, F., MacDonald, L.A., Turner, K.W., Thienpont, J.R., Medeiros, A.S., Biskaborn, B.K., ... Wolfe, B.B., 2017. Paleolimnology of thermokarst lakes: a window into permafrost landscape evolution. Arctic Sci 3 (2), 91–117.

Box, J.E., Colgan, W.T., Christensen, T.R., Schmidt, N.M., Lund, M., Parmentier, F.J.W., Walsh, J.E., 2019. Key indicators of Arctic climate change: 1971–2017. Environ. Res. Lett. 14 (4), 045010.

Burn, C.R., 1997. Cryostratigraphy, paleogeography, and climate change during the early Holocene warm interval, western Arctic coast, Canada. Can. J. Earth Sci. 34, 912–925.

Burn, C.R., 2002. Tundra lakes and permafrost, Richards Island, western Arctic coast, Canada. Can. J. Earth Sci. 39, 1281–1298. https://doi.org/10.1139/e02-035.

Burn, C.R., Kokelj, S.V., 2009. The environment and permafrost of the Mackenzie Delta area. Permafrost Periglac. 20, 83–105 (doi.org/10.1002).

Connon, R.F., Quinton, W.L., Craig, J.R., Hayashi, M., 2014. Changing hydrologic connectivity due to permafrost thaw in the lower Liard River valley, NWT, Canada. Hydrol. Process. 28 (14), 4163–4178.

Craig, H., 1961. Isotopic variations in meteoric waters. Science 133, 1702–1703.

Craig, H., Gordon, L.I., 1965. Deuterium and oxygen 18 variations in the ocean and the marine atmosphere. In: Tongiorgi, E. (Ed.), Stable Isotope in Oceanographic Studies and Paleotemperatures. Laboratorio di Geologia Nucleare, Pisa, Italy, pp. 9–130.

Deison, R., Smol, J.P., Kokelj, S.V., Pisaric, M.F., Kimpe, L.E., Poulain, A.J., … Blais, J.M., 2012. Spatial and temporal assessment of mercury and organic matter in thermokarst affected lakes of the Mackenzie Delta Uplands, NT, Canada. Environ. Science Tech. 46 (16), 8748–8755.

Eickmeyer, D.C., Kimpe, L.E., Kokelj, S.V., Pisaric, M.F., Smol, J.P., Sanei, H., ... Blais, J.M., 2016. Interactions of polychlorinated biphenyls and organochlorine pesticides with sedimentary organic matter of retrogressive thaw slump-affected lakes in the tundra uplands adjacent to the Mackenzie Delta, NT, Canada. J. Geophys. Res.: Biogeosciences 121 (2), 411–421.

Environment and Climate Change Canada, 2019. 1981-2010 climate normals and averages. Accessed 27 Feb 2020. https://climate.weather.gc.ca/climate_normals/index_e.html.

Gibson, J.J., 2002. Short-term evaporation and water budget comparisons in shallow Arctic lakes using non-steady isotope mass balance. J. Hydrol. 264 (1–4), 242–261.

Gibson, J.J., Edwards, T.W.D., 2002. Regional water balance trends and evaporation-transpiration partitioning from a stable isotope survey of lakes in northern Canada. Glob. Biogeochem. Cycles 16 (2), 10–11.

Gibson, J.J., Edwards, T.W.D., Bursey, G.G., Prowse, T.D., 1993. Estimating evaporation using stable isotopes: quantitative results and sensitivity analysis for two catchments in northern Canada. Nordic Hydrol 24, 79–94.

Gibson, J.J., Birks, S.J., Edwards, T.W.D., 2008. Global prediction of δ_A and δ^2H-$\delta^{18}O$ evaporation slopes for lakes and soil water accounting for seasonality. Glob. Biogeochem. Cycles 22 (2), GB2031. https://doi.org/10.1029/2007GB002997.

Gibson, J.J., Birks, S.J., Jeffries, D.S., Kumar, S., Scott, K.A., Aherne, J., Shaw, P., 2010. Site-specific estimates of water yield applied in regional acid sensitivity surveys in western Canada. J. Limnol. 69 (Suppl. 1), 67–76. https://doi.org/10.4081/jlimnol.2010.s1.67.

Gibson, J.J., Birks, S.J., Yi, Y., Vitt, D., 2015. Runoff to boreal lakes linked to land cover, watershed morphology and permafrost thaw: a 9-year isotope mass balance assessment. Hydrol. Process. 29 (18), 3848–3861.

Gibson, J.J., Birks, S.J., Yi, Y., 2016a. Stable isotope mass balance of lakes: a contemporary perspective. Quaternary Sci. Rev. 131 (B), 316–328.

Gibson, J.J., Birks, S.J., Yi, Y., Moncur, M.C., McEachern, P.M., 2016b. Stable isotope mass balance of fifty lakes in central Alberta: assessing the role of water balance and climate in determining trophic status and lake level. J. Hydrol.: Reg. Stud. 6, 13–25.

Gibson, J.J., Birks, S.J., Jeffries, D., Yi, Y., 2017. Regional trends in evaporation loss and water yield based on isotope mass balance of lakes: the Ontario Precambrian Shield surveys. J. Hydrol. 544, 500–510.

Gibson, J.J., Birks, S.J., Yi, Y., Shaw, P., Moncur, M.C., 2018. Isotopic and geochemical surveys of lakes in coastal BC: insights into regional water balance and water quality controls. J. Hydrol.: Reg. Stud. 17, 47–63.

Gibson, J.J., Birks, S.J., Moncur, M.C., 2019a. Mapping water yield distribution across the southern Athabasca Oil Sands area: baseline surveys applying isotope mass balance of lakes. J. Hydrol.: Reg. Stud. 21, 1–13.

Gibson, J.J., Yi, Y., Birks, S.J., 2019b. Isotopic tracing of hydrologic drivers including permafrost thaw status for lakes across northeastern Alberta, Canada: a 16-year, 50-lake perspective. J. Hydrol.: Reg. Stud. 26, 100643. https://doi.org/10.1016/j.ejrh.2019.100643.

Hinzman, L.D., Bettez, N.D., Bolton, W.R., Chapin, F.S., Dyurgerov, M.B., Fastie, C.L., Yoshikawa, K., 2005. Evidence and implications of recent climate change in Northern Alaska and other Arctic regions. Clim. Chang. 72 (3), 251–298.

Horita, J., Wesolowski, D., 1994. Liquid-vapour fractionation of oxygen and hydrogen isotopes of water from the freezing to the critical temperature. Geochim. Cosmochim. Acta 58, 3425–3437. https://doi.org/10.1016/0016-7037(94)90096-5.

Horita, J., Rozanski, K., Cohen, S., 2008. Isotope effects in the evaporation of water: a status report of the Craig-Gordon model. Isot. Environ. Health Stud. 44, 23e49.

Houben, A.J., French, T.D., Kokelj, S.V., Wang, X., Smol, J.P., Blais, J.M., 2016. The impacts of permafrost thaw slump events on limnological variables in upland tundra lakes, Mackenzie Delta region. Fund. Appl. Limnol. 189 (1), 11–35.

IAEA, International Atomic Energy Agency, 2011. Fourth Interlaboratory Comparison Exercise for δ^2H and $\delta^{18}O$ Analysis of Water Samples (WICO 2011). Isotope Hydrology Section, International Atomic Energy Agency, Vienna (67pp).

Karlsson, J., Giesler, R., Persson, J., Lundin, E., 2013. High emission of carbon dioxide and methane during ice thaw in high latitude lakes: carbon emission from lakes in spring. Geophys. Res. Lett. 40, 1123–1127.

Kettles, I.M., Tarnocai, C., 1999. Development of a model for estimating the sensitivity of Canadian peatlands to climate warning. Geogr. Phys. Quat. 53, 323–338.

Kokelj, S.V., Jorgenson, M.T., 2013. Advances in thermokarst research. Permafrost Periglac. Process. 24 (2), 108–119.

Kokelj, S.V., Jenkins, R.E., Milburn, D., Burn, C.R., Snow, N., 2005. The influence of thermokarst disturbance on the water quality of small upland lakes, Mackenzie Delta Region, Northwest Territories, Canada. Permafrost Periglac. Process. 16, 343–353.

Kokelj, S.V., Zajdlik, B., Thompson, M.S., 2009. The impacts of thawing permafrost on the chemistry of lakes across the subarctic boreal-tundra transition, Mackenzie Delta Region. Permafrost Periglac. Process. 20, 185–199.

Kokelj, S.V., Tunnicliffe, J., Lacelle, D., Lantz, T.C., Chin, K.S., Fraser, R., 2015. Increased precipitation drives mega slump development and destabilization of ice-rich permafrost terrain, northwestern Canada. Global Planetary Change 129, 56–68.

Kokelj, S.V., Palmer, M.J., Lantz, T.C., Burn, C.R., 2017. Ground temperatures and permafrost warming from forest to tundra, Tuktoyaktuk coastlands and Anderson Plain, NWT, Canada. Permafrost Periglac. Process. 28, 543–551 doi.org/10.1002.

Lacelle, D., Bjornson, J., Lauriol, B., Clark, I.D., Troutet, Y., 2004. Segregated-intrusive ice of subglacial meltwater origin in retrogressive thaw flow headwalls, Richardson Mountains, NWT, Canada. Quat. Sci. Rev. 23 (5–6), 681–696.

Lacelle, D., Bjornson, J., Lauriol, B., 2009. Climatic and geomorphic factors affecting contemporary (1950–2004) activity of retrogressive thaw slumps on the Aklavik plateau, Richardson Mountains, NWT, Canada. Permafrost Periglac. Process. 21, 1–15.

Lacelle, D., Fontaine, M., Forest, A.P., Kokelj, S., 2013. High-resolution stable water isotopes as tracers of thaw unconformities in permafrost: a case study from western Arctic Canada. Chem. Geol. 368, 85–96.

Lacelle, D., Brooker, A., Fraser, R.H., Kokelj, S.V., 2015. Distribution and growth of thaw slumps in the Richardson Mountains-Peel Plateau region, northwestern Canada. Geomorphology 235, 40–51.

Landha¨usser, S.M., Wein, R.W., 1993. Postfire vegetation recovery and tree establishment at the Arctic treeline: climate-change-vegetation-response hypotheses. J. Ecol. 81, 665–672.

Lansard, B., Mucci, A., Miller, L.A., MacDonald, R.W., Gratton, Y., 2012. Seasonal variability of water mass distribution in the southeastern Beaufort Sea determined by total alkalinity and $\delta^{18}O$. J. Geophys. Res.: Oceans 117 (3), 1–19.

Lantuit, H., Pollard, W.H., Couture, N., Fritz, M., Schirrmeister, L., Meyer, H., Hubberten, H.W., 2012. Modern and late Holocene retrogressive thaw slump activity on the Yukon Coastal Plain and Herschel Island, Yukon Territory, Canada. Permafrost Periglac. Process. 23, 39–51.

Lantz, T.C., Kokelj, S.V., 2008. Increasing rates of retrogressive thaw slump activity in the Mackenzie Delta region, N.W.T. Canada. Geophys. Res. Lett. 35, L06502.

Lantz, T.C., Turner, K.W., 2015. Changes in lake area in response to thermokarst processes and climate in Old Crow Flats, Yukon. J. Geophys. Res. Biogeosci. 120 (3), 513–524. https://doi.org/10.1002/2014JG002744.

Lantz, T.C., Marsh, P., Kokelj, S.V., 2013. Recent shrub proliferation in the Mackenzie Delta uplands and microclimatic implications. Ecosystems 16 (1), 47–59.

Leng, M.J., Anderson, N.J., 2003. Isotopic variation in modern lake waters from western Greenland. The Holocene 13 (4), 605–611. https://doi.org/10.1191/0959683603hl620rr.

Lewkowicz, A.G., Way, R.G., 2019. Extremes of summer climate trigger thousands of thermokarst landslides in a high Arctic environment. Nat. Commun. 10 (1), 1–11.

Liljedahl, A.K., Boike, J., Daanen, R.P., Fedorov, A.N., Frost, G.V., Grosse, G., Zona, D., 2016. Pan-Arctic ice-wedge degradation in warming permafrost and its influence on tundra hydrology. Nat. Geosci. 9 (4), 312–318.

Luo, J., Niu, F., Lin, Z., Liu, M., Yin, G., 2019. Recent acceleration of thaw slumping in permafrost terrain of Qinghai-Tibet Plateau: An example from the Beiluhe Region. Geomorphology 341, 79–85.

MacDonald, L.A., Wolfe, B.B., Turner, K.W., Anderson, L., Arp, C.D., Birks, S.J., ... McDonald, I., 2016. A synthesis of thermokarst lake water balance in high-latitude regions of North America from isotope tracers. Arctic Sci 3 (2), 118–149.

Mackay, J.R., 1995. Active layer changes (1968 to 1993) following the forest-tundra fire near Inuvik, NWT, Canada. Arctic Alpine Res 27 (4), 323–336.

Mann, P.J., Spencer, R.G.M., Hernes, P.J., Six, J., Aiken, G.R, Tank, S.E., …, Holmes, R.M., 2016. Pan-Arctic trends in terrestrial dissolved organic matter from optical measurements. Front. Earth Sci. 4, 25. doi: https://doi.org/10.3389/feart.2016.00025.

Marsh, P., Russell, M., Pohl, S., Haywood, H., Onclin, C., 2009. Changes in thaw lake drainage in the Western Canadian Arctic from 1950 to 2000. Hydrol. Process. 23, 145–158.

Mesinger, F., DiMego, G., Kalnay, E., Mitchell, K., Shafran, P.C., Ebisuzaki, W., ... Shi, W., 2006. North American Regional Reanalysis: a long-term, consistent, high-resolution climate dataset for the North American domain, as a major improvement upon the earlier global reanalysis datasets in both resolution and accuracy. Bull. Am. Meteorol. Soc. 87, 343–360.

Mesquita, P.S., Wrona, F.J., Prowse, T.D., 2010. Effects of retrogressive permafrost thaw slumping on sediment chemistry and submerged macrophytes in Arctic tundra lakes. Freshw. Biol. 55 (11), 2347–2358.

Narancic, B., Wolfe, B.B., Pienitz, R., Meyer, H., Lamhonwah, D., 2017. Landscape-gradient assessment of thermokarst lake hydrology using water isotope tracers. J. Hydrol. 545, 327–338.

Pavlov, A.V., 1994. Current changes of climate and permafrost in the arctic and sub-arctic of Russia. Permafrost Periglac. Process. 5 (2), 101–110.

Rampton, V.N., 1988. Quaternary geology of the Tuktoyaktuk coastlands, Northwest Territories. Geological Survey of Canada, Memoir 423. https://doi.org/10.4095/12693798pp.

Ritchie, J.C., 1984. Past and Present Vegetation of the Far Northwest of Canada. University of Toronto Press, Toronto https://doi.org/10.1016/0033-5894(86)90065-7 251pp.

Séjourné, A., Costard, F., Fedorov, A., Gargani, J., Skorve, J., Massé, M., Mège, D., 2015. Evolution of the banks of thermokarst lakes in Central Yakutia (Central Siberia) due to retrogressive thaw slump activity controlled by insolation. Geomorphology 241, 31–40.

Thienpont, J.R., Kokelj, S.V., Korosi, J.B., Cheng, E.S., Desjardins, C., Kimpe, L.E., Smol, J.P., 2013. Exploratory hydrocarbon drilling impacts to Arctic lake ecosystems. PLoS One 8, e78875.

Thompson, M.S., Wrona, F.J., Prowse, T.D., 2012. Shifts in plankton, nutrient and light relationships in small tundra lakes caused by localized permafrost thaw. Arctic 65, 367–376.

Timoney, K.P., Laroi, G.H., Zoltai, S.C., Robinson, A.L., 1992. The high sub-arctic forest-tundra of northwestern Canada - position, width, and vegetation gradients in relation to climate. Arctic 45, 1–9.

Tondu, J.M.E., Turner, K.W., Wolfe, B.B., Hall, R.I., Edwards, T.W.D., McDonald, I., 2013. Using water isotope tracers to develop the hydrological component of a long-term aquatic ecosystem monitoring program for a northern lake-rich landscape. Arct. Antarct. Alp. Res. 45 (4), 594–614. https://doi.org/10.1657/1938-4246-45.4.594.

Turner, K.W., Wolfe, B.B., Edwards, T.W.D., 2010. Characterizing the role of hydrological processes on lake water balances in the Old Crow Flats, Yukon Territory, Canada, using water isotope tracers. J. Hydrol. 386 (1–4), 103–117. https://doi.org/10.1016/j.jhydrol.2010.03.012.

Turner, K.W., Wolfe, B.B., Edwards, T.W.D., Lantz, T.C., Hall, R.I., Larocque, G., 2014. Controls on water balance of shallow thermokarst lakes and their relations with catchment characteristics: a multi-year, landscape-scale assessment based on water isotope tracers and remote sensing in Old Crow Flats, Yukon (Canada). Glob. Chang. Biol. 20 (5), 1585–1603.

Vonk, J.E., Tank, S.E., Bowden, W.B., Laurion, I., Alekseychik, P., Amyot, M., Wickland, K.P., 2015. Reviews and syntheses: effects of permafrost thaw on Arctic aquatic ecosystems. Biogeosciences 12, 7129–7167.

Wan, C., Gibson, J.J., Shen, S., Yi, Y., Yi, P., Yu, Z., 2019. Using stable isotopes paired with tritium analysis to assess thermokarst lake water balances in the Source Area of the Yellow River, northeastern Qinghai-Tibet Plateau, China. Sci.Total Environ. 689, 1276–1292.